CERN-SPSC-2013-009
(SPSC-SR-115)
21.03.2013

2013 NA62 Status Report to the CERN SPSC

Abstract

NA62 aims to study the rare decay $K^+ \to \pi^+\nu\bar{\nu}$ at the CERN SPS. In this document we report the status of the detector construction and the general progress of the experiment since April 2012. A report on the achievements obtained during the 2012 technical run is given. The schedule for the completion of the construction and the preparations in view of the physics data taking in October 2014 are detailed.

Contents

1 Introduction

The main aim of NA62 is to measure precisely the branching ratio of the very rare decay $K^+ \to \pi^+\nu\bar{\nu}$, a decay sensitive to new physics [1] via loop processes and well predicted in the Standard Model (SM) [2]. NA62 plans to improve the current experimental precision [3] $B(K^+ \to \pi^+\nu\bar{\nu}) = (1.73^{+1.15}_{-1.05}) \times 10^{-10}$ exploiting a novel decay-in-flight

technique based on calorimetry to veto extra particles, very light mass trackers to reconstruct the K^+ and the π^+ momenta and full particle identification capability. Generally speaking, during the past year we have witnessed important progress in the study of quark and lepton flavour. The LHCb experiment has reported [4] the first evidence for $B^0_{(s)} \to \mu^+\mu^-$. The result, $BR(B^0_{(s)} \to \mu^+\mu^-) = (3.2^{+1.5}_{-1.2}) \times 10^{-9}$, is in good agreement with the theoretical SM expectation. Evidence [5] of CP-Violation in D meson decays was not confirmed [6]. On the lepton flavour sector, the MEG Collaboration has reported a new incisive upper limit [7] on $\mu^+ \to e^+\gamma$ while NA62 has published its final result on lepton universality in charged K decays [8].

2 Technical Co-ordination and Schedule

During the past 12 months good progress was made on the infrastructure in the experimental area and the technical services. A very noticeable event has been the installation of the new overhead crane in ECN3 which was accomplished in February 2013. The renovation work in the surface building is by now mostly completed, except for the cooling system of the PC-Farm racks which will be done in the course of 2013. At the same time the collaboration has brought forward the detector installation as foreseen in our last report one year ago (Fig. 1). A particular highlight was, in September 2012, the installation of the first Straw chamber, with Module 1 fully equipped with straws (see Fig. 2). The overall installation status and the operation conditions during the technical run (TR) are summarised in Table 1. Fig. 3 shows the comparison between the detector used in the TR and the final layout of the experiment. This gives a first overview of the work that still is to be completed in next the 18 months.

The TR took place from October 29 to December 3, 2012 and shifts were run around the clock during the 5-week period. The 105 8-hour shifts were covered by two persons each, 80 enthusiastic shifters coming from 26 Institutes of the NA62 Collaboration. In addition, DAQ, trigger, DCS and sub-detector experts were fully dedicated to the run together with the respective coordinators. The TR was not only a great opportunity to put together the different components of the detector but also a true occasion of integrating newcomers and fostering the Collaboration spirit.

2.1 Plans until October 2014

Based on the experience gained last year, we are confident that it is realistic to install the remaining detectors for a first physics run starting in October 2014. The installation schedule of the detectors is shown in Fig. 4. However, the detector construction is still on-going and numerous technical challenges are still in front of us. In this context, we think that the following items are the most critical for the schedule:

- GTK: the submission of the final ASIC design for fabrication is about to happen. In parallel we are tendering for chip thinning and flip-chip bonding. The remaining work, including the readout, is technically difficult with a tight time plan, but we believe that it is feasible to complete a first version of full size detectors for the physics run in October 2014.

- Straw Tracker: the rate of the module assembly has improved significantly and is proceeding well on both production sites (CERN and Dubna). The straw production in Dubna has sufficient capacity to keep up in speed with the module assembly.

Sub-System	Installation	Operation in Technical Run
CEDAR/KTAG	The CEDAR and the KTAG were installed. Four (out of eight) ϕ sectors equipped to 50% with photodetectors	All four sectors operational and read out. Time synchronization, pressure scan and detector alignment were done successfully.
GTK	*Was not installed for the TR*	A Si wafer was placed in the beam to emulate the GTK effect on rates
CHANTI	A prototype detector used with and without vacuum (positioned near LAV A1 to use common read out rack)	Readout of all 46 channels (up to 32 channels simultaneously)
STRAW	Chamber 1 installed with two Modules u/v: Straws/Wires fully equipped; x/y: empty frame (no straws) made vacuum tight	Read out was limited to eight front end boards with two SRB prototype boards
LAV	Eight LAV detectors were installed, three were fully connected to the HV and LV supplies as well as readout crates	LAV A1, A2 and A3 were included in the readout
RICH	*Was not installed for the TR*	
CHOD/NHOD	The NA48 CHOD and NHOD were reconditioned and equipped with the LAV Frontend boards Several small prototypes for future CHOD upgrade were installed and tested	CHOD and NHOD were read out and used for the trigger
IRC	*Was not installed for the TR*	
LKr	Detector fully installed	Read out with CPD / SLM system (limited to about 40% of the channels by the availability of FASTBUS power supplies)
MUV	MUV2 and MUV3 fully installed	Both modules were fully used (also in the trigger)
SAC	Final detector installed; provisional read out	TDC read-out based on LAV Front End boards. Standalone tests with a commercial CAEN 1 GHz FADC
Vacuum Tank vacuum system	85 m (out of 115 m in total) vacuum tank and corresponding detector elements were installed. The primary pumping system and three (out of seven) cryopumps were installed	The leak tightness of the tank and the LAV detectors was at the expected level. Vacuum pressure reached 10^{-5} mbar with one pump and 4×10^{-6} mbar with two cryopumps

Table 1: Summary of the sub-systems installed and used in the TR

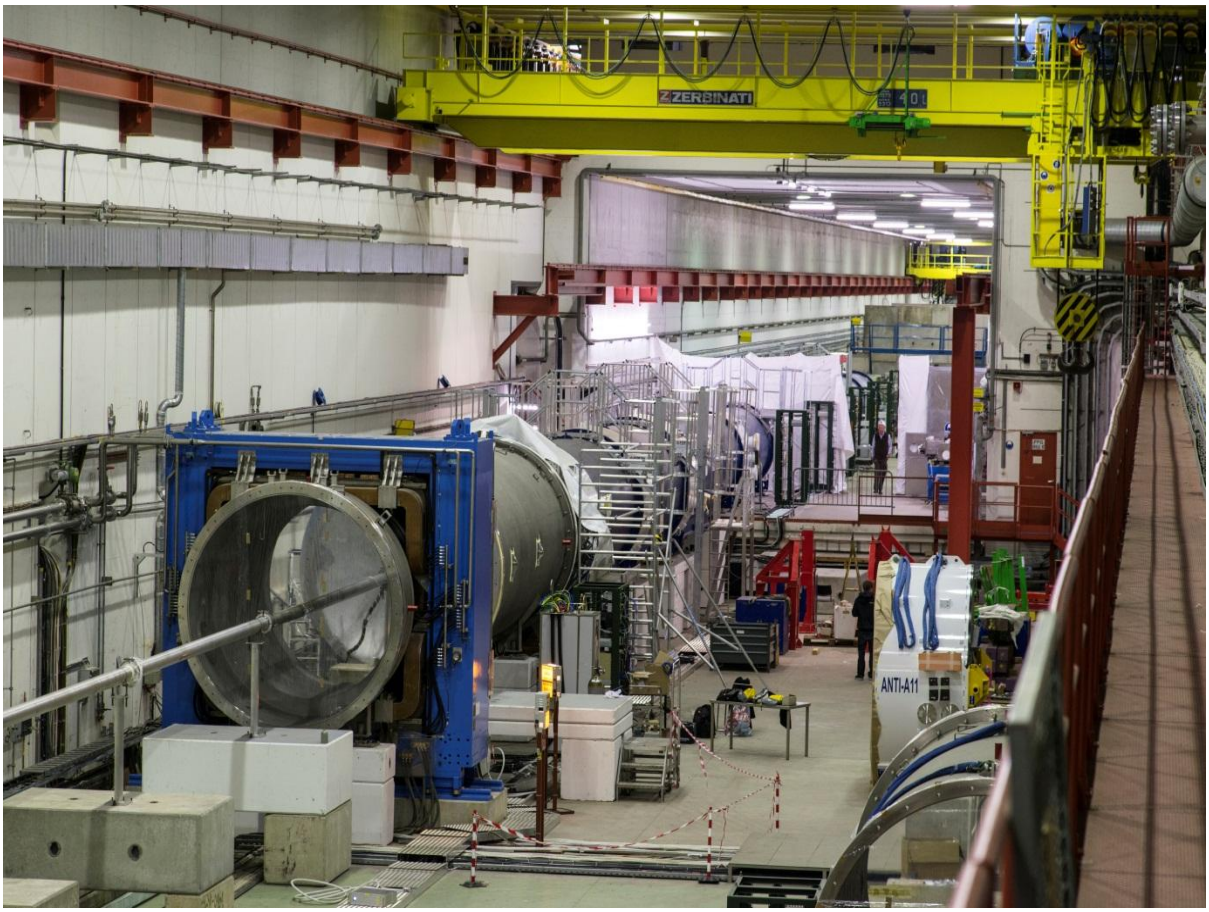

Figure 1: NA62 experimental area during the installation in October 2012

Limited resources on the electronics have been a bottleneck in the preparation of the TR and they continue to be problematic. At this stage, we give high priority to the work on the frontend cover allowing us to equip the covers in time when stacking the modules. The SRB (back-end) development and tests will continue until early 2014.

- RICH: the subcontractor for the RICH vessel is making good progress and we look forward to receive it as foreseen in autumn this year. The spherical glass substrates for the mirrors are at CERN and the aluminium coating will start in spring this year. The fabrication of the mirror support panel as well as the design work for the mirror mounts are on the critical path.

- LKr / CREAM readout: CAEN has announced delivery of the final CREAM prototypes in the course of March, and gave us positive feedback on their progress for hardware and firmware. The planning foresees the delivery of all modules between December 2013 and March 2014.

- Infrastructure: we have started in January 2013 to prepare tenders for the remaining vacuum tanks (tanks ♯ 26 and ♯ 28), the straw interface pieces and the aluminium beam pipe for the RICH.

Figure 2: First Straw Chamber coming down the pit a few days before the installation in the experiment

3 The installation and commissioning of the new beam line

The old K12 beam line providing simultaneous K^+ and K^- beams to the NA48/2 experiment was dismounted in 2011 and, apart from the T10 production target for the K12 beam and the Liquid Krypton calorimeter (LKr), all equipment was removed from the beam line. The exact positions of the target and the calorimeter were re-measured by the survey team and small offsets compared to the original positions were observed. The nominal axis of the new K12 beam was defined to pass through the centres of the T10 target and the LKr calorimeter. The last section of the P42 beam, starting from the switching magnets between the P42+K12 and the now mostly dismounted P41+H10 lines was realigned to match the new beam axis and the switching magnets themselves aligned on the P42 axis, rather than on the bisector between P41 and P42. This realignment affected 15 magnets plus beam instrumentation. Also in 2011 the 132 tons spectrometer magnet MNP33 was moved to its new location, about 30 m further upstream and aligned on the new beam axis.

The installation of the K12 beam line itself started towards the middle of 2012. The beam optics of the beam line upstream of the blue tube is shown in Fig. 5. This part of the beam line contains eight dipole magnets, five corrector dipoles, ten quadrupoles, three dipole muon sweepers and a magnetic collimator with toroidal field. Additionally there

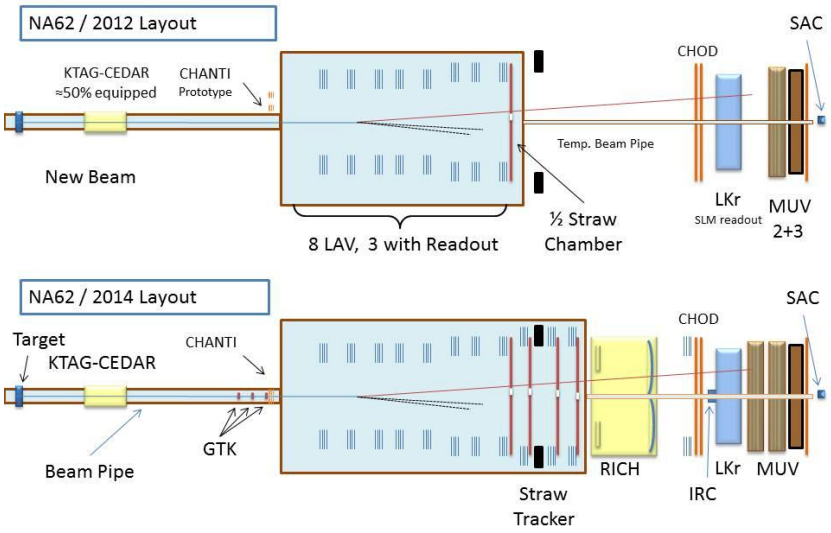

Figure 3: Schematic comparison of the detector layout used in the TR and the final layout

are two motorised TAX dump-collimators, three two-jaw and two four-jaw collimators, a radiator to reduce the e^+ content in the beam and three pairs of FISC filament scanners; it also houses the modified CEDAR counter (with its new Cerenkov light detection system called KTAG). The distance between the T10 target centre and the start of the blue tank is about 105 m. The TAXs are motorised via a 5 m long axle, allowing the motors to be located sideways behind the shielding. Therefore the motors can be repaired now with strongly reduced radiation dose to the personnel. The beam line is under continuous vacuum with the exception of the passage through the TAXs and the CEDAR counter which is separated from the vacuum by single hydro-formed aluminium windows at each end of 150 μm thickness upstream and 200 μm downstream. In

Fig. 6 a) and b) we show, respectively, a picture of the beam line under construction and a view of the frontend of the new beam line just before the installation of the roof shielding. During the TR the frontend, from the T10 target up to QUAD04, was completely shielded on the sides and on top. The beam line feeds directly via a gate valve into the blue tank that serves as decay volume. For the TR the decay tank was only installed up to Straw 1, which was half equipped with straws. From there the decay tank was closed with a hydro-formed aluminium window of 4 mm thickness, reused from NA48 and NA48/2, with a central hole connecting to a 159 mm standard vacuum tube up to the LKr calorimeter and traversing the MNP33 spectrometer magnet. The beam then traverses a complex set of vacuum tubes, the various detectors and finally the MBPL-TP dipole magnet that sweeps away the charged beam from the neutral decay products that are tagged by the SAC veto counter. This detector is housed inside a 60 cm diameter

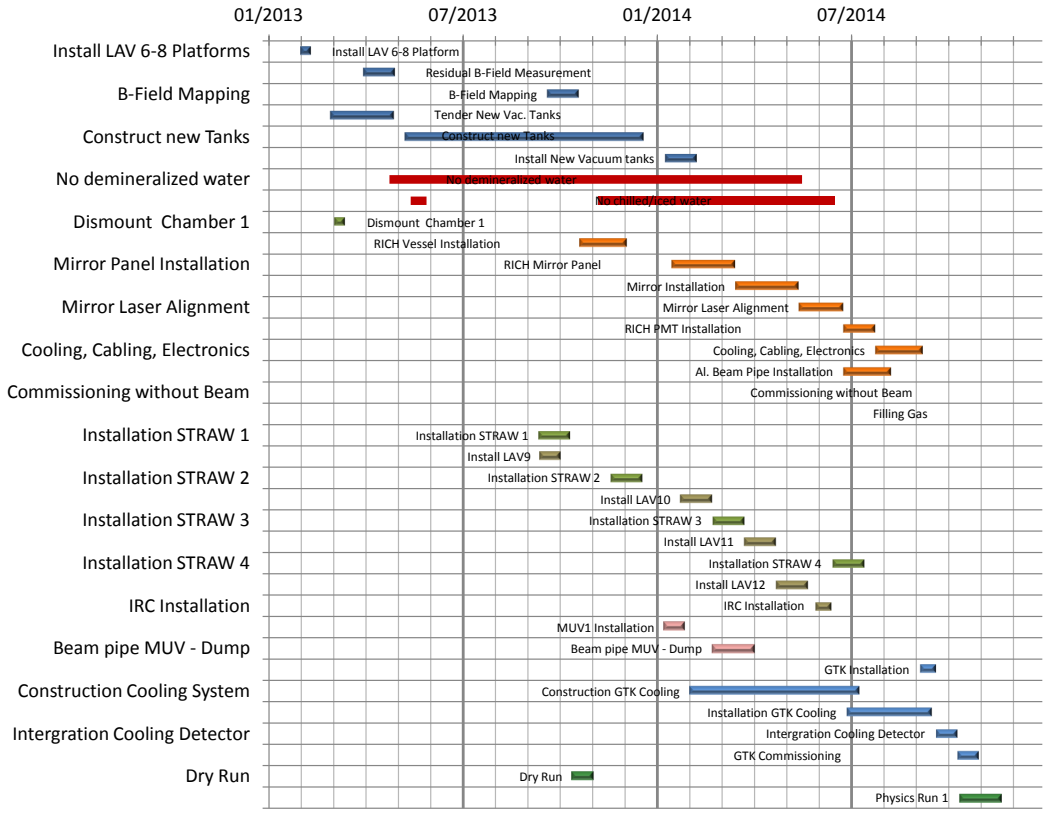

Figure 4: Installation Schedule until October 2014

vacuum tank located in the new tunnel, installed 24 m below ground and leading to the new beam dump.

In this final sector of the beam a special "Big FISC" filament scanner has been prepared with a larger scanning range. This new device was completed just in time for the start of the TR. The beam vacuum is assured by two rotary-vane pumps in the sector between the T10 target and the TAX, three rotary-vane pumps between TAX and CEDAR, four turbo pumps between the CEDAR and the start of the blue tank and three turbo pumps in the sector behind the blue tank. Upstream of the CEDAR the vacuum pressure is at the 10^{-3} mbar level, between the CEDAR and the blue tank, as well as downstream of the LKR calorimeter it is better than 5 $\times 10^{-4}$ mbar. For the blue tank itself, three cryopumps [9] and a roughing pump were installed, but usually only one or two cryopumps were in operation. In spite of some small leaks vacuum levels consistent with the expectations and more than adequate for the TR were achieved. For the moment the system was operated manually from TCC8 and ECN3.

The operation of the beam line also required some upgrades and modifications of the infrastructure. The cooling station for the T10 target station was obsolete, highly activated and located next to the target itself. It had to be replaced by a new cooling station located in the access gallery from the TCC8 access shaft to the TCC8 target zone itself. This cooling system with the interlock on the beam was commissioned in the second half of October 2012.

The access shafts from the control room down to the ECN3 underground cavern (PPG853 an 854) were isolated from the cavern itself by air locks at the ECN3 end. In

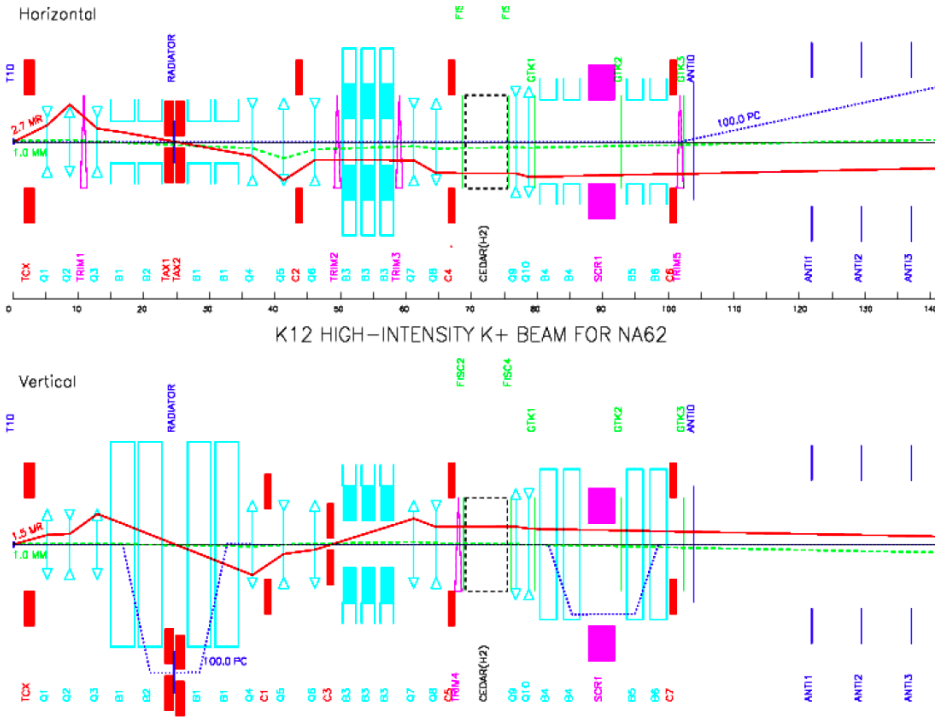

Figure 5: The optics of the K12 beam line for NA62

case of failure of the pumps of the air locks an alarm was raised in the CCC.

The control rooms in the B918 surface building were completely refurbished and reorganised, taking advantage of the fact that the NA60 experiment had been dismantled and the space of their control room liberated for NA62. Most of the obsolete infrastructure in the building has been renovated, in particular the cooling and ventilation systems and the electrical infrastructure. In addition to a comfortable control room and a PC farm room, there is a meeting room. This work was completed well ahead of the start of the TR, in spite of some damage to the building caused by the backfilling of the earth after the civil engineering work for the beam dump. The radiation monitoring system was upgraded from the obsolete ARCON system to the new RAMSES system. The installation for the monitoring of the extracted air is planned together with the installation of the new ventilation system in 2015. Finally, all beam line and relevant interlock systems were integrated in the Cesar beam control system. The beam line installation was completed on Wednesday, October 31, and the Beam Permit was signed on the morning of November 1.

3.1 Commissioning and performance of the beam line

The beam line being in its final form, one of the important objectives of the TR was the full commissioning of the K12 beam line and the evaluation of its performance. The only limitation was the non-availability of the new ventilation systems in TCC8, ECN3 and GL300 and in particular the absence of an adequate separation between the different air

a) b)

Figure 6: a) Picture of the installation of the new beam line; b) The frontend of the beam line, just before the installation of the top shielding

volumes. Any access to ECN3 would thus require long cool-down times after operation at high intensities. Therefore we restricted the intensity incident on the T10 target to well below 10% of nominal for most of the period and we only exceeded this value on the last weekend. For reasons related to the NA62 requirements as well as to avoid an impact on the other North Area users, we never exceeded 15% of the nominal proton flux incident on T10. However, the K12 beam itself was operated at its nominal settings in the last part of the TR.

In the afternoon of November 1 the 838 metres long P42 beam line, which had not operated since 2009, was put back in operation and after a few hours the primary beam was centred on the 2 mm diameter T10 target and the beam was well aligned in all collimators. Only the passage through the P42 TAX will require some further optimisation at some stage, but this was postponed till 2014 because the tuning would have perturbed the H6 and H8 users in this very busy last part of the 2012 run and because anyway T4 and the P42 TAX will be worked on during the long shutdown 1 (LS1). A beam of muons could be provided to NA62 already in this first night.

On November 2 in the afternoon the new K12 beam was switched on with nominal currents, but collimators closed to 10% of their nominal aperture ("pencil beam") and already in the first burst a profile was seen at the end of the beam line, in the analogue MWPC wire chamber just upstream of the final beam dump. This first spill is shown in Fig. 7. The profile was only slightly off-centred and the intensity was already close to the expectation for these collimator settings. Due to a number of machine development

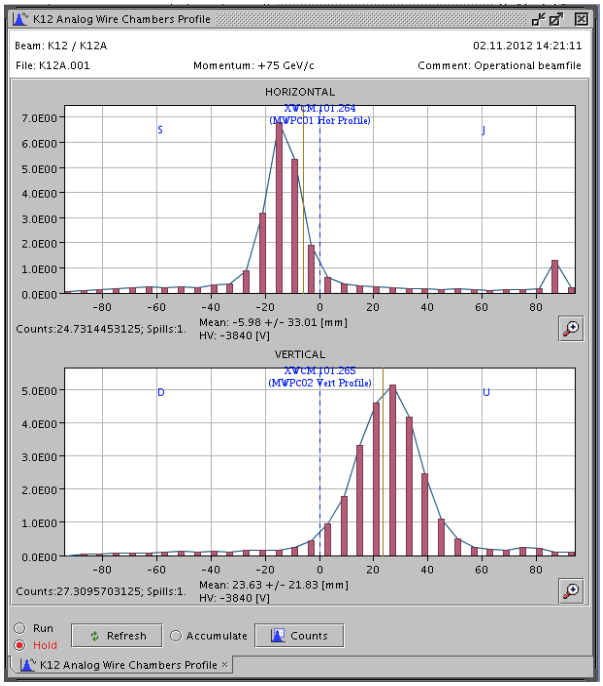

Figure 7: The first profile observed at the end of the K12 beam (pencil beam)

(MD) sessions, flooding problems in the SPS ring and in TCC8 and ECN3, various other machine problems and the NA62 request for muon beams, kaon beam tuning essentially resumed only on November 16. The pencil beam tuning was completed, without any problem on that same day, after a careful final tuning of the filament scanners by the Beam Instrumentation team.

On November 22 the tuning of the full acceptance K12 beam started. On that day an attempt was made to optimise the transmission from the T10 production target through the TAX, by tuning the three QNRB-type quadrupoles. Quite large offsets in currents were observed, in particular for the second QNRB, and the beam shape downstream of the TAX looked incorrect. On November 24, at the next attempt, the problem was understood to be a combination of an inversion of the horizontal and vertical 4-jaw collimators (which had not cut the beam in the pencil beam mode) and a bad description of the integrated gradient (GL) versus current (I) curve of QNRB quadrupoles in saturation. After the run we received new GL measurements and a new fit was made, shown in Fig. 8. The difference between the old and new curves explains the current difference qualitatively and quantitatively. The fine tuning of the K12 beam could be completed on the weekend of November 24 and 25. The last week of the run was left for beam cleanliness measurements and NA62 trigger, detector and data acquisition studies. An indicative summary of the use of beam time during the TR is shown in Fig. 9.

As an illustration of the quality of the beam we show in Fig. 10 the profiles measured with the Big Fiscs, located behind the LKr calorimeter in the MUV region of the detector.

A number of studies were made to address the amount of tails in the beam profile

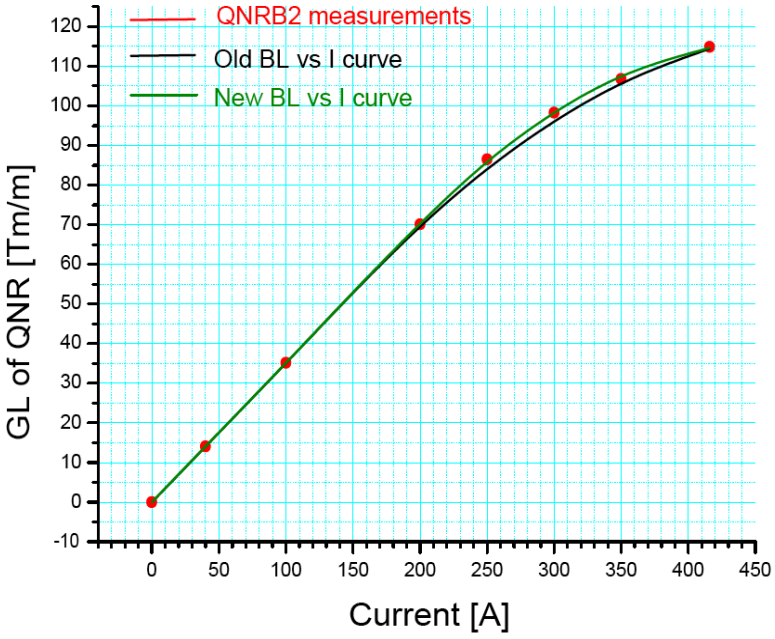

Figure 8: The new and old fits to the integrated gradient GL of QNRB quadrupoles against the current I

and the effect of material on them. In particular the effect of the material of the CEDAR and of the GTK was evaluated. For different configurations the increase of counting rate was observed in the Straw 1 detector. A comparison of the rates in the straw closest to the beam showed an increase by a factor of 1.6 when a 380 μm thick silicon plate was inserted on the beam at the level of GTK3. Emptying the CEDAR from its Nitrogen (5 m of N_2 at 1.7 bar absolute pressure) reduced the RMS of the beam at the straw by about 2 mm, as expected. These measurements are shown in Fig. 11 and they are consistently confirmed by other observations.

3.2 Remaining work on the beam line

The beam line has performed satisfactorily. As a result of the TR the alignment of the QNRB quadrupoles will be verified in situ. The last of the four frontend achromat MTR magnets will be rotated by 180° to ease the access to its connections via an existing access chicane in the shielding. In that same region minor improvements will be made to the side shielding around the TAX. The control of horizontal and vertical jaws of the 4-jaw collimators will be corrected. In the 2014 run the steering through the TAX will be redone, this time with the correct downstream collimator apertures. The T10 target itself will be thoroughly consolidated during LS1 and realigned subsequently.

The infrastructure in the TCC8 and ECN3 caverns still needs more work. During the TR we could not run at nominal rate on the T10 target, because the lack of an

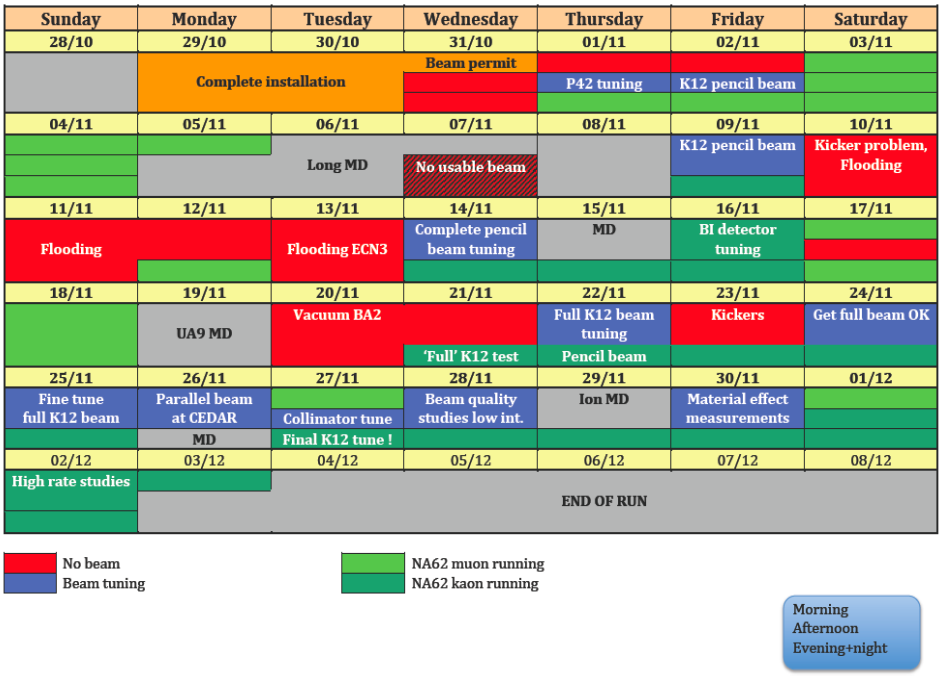

Figure 9: An overview of the use of beam time during the TR. Beam tuning sessions are indicated in blue. Beam for the experiment in green

adequate ventilation system would lead to long cool-down times before any access into ECN3. The installation of the new ventilation relies on an air-tight separation between the air volumes of the TCC8 target cavern and the ECN3 part of the complex where the NA62 detectors are installed. This separation will be made in the form of a double wall (air lock) with over-pressure in between. A view of the present design is shown in Fig. 12.

These walls can be opened "easily" in case the crane has to pass this wall. This procedure will take a number of hours, but it is expected to happen only rarely and in such cases the access to the activated equipment in TCC8 anyway requires some cool-down time. During beam operation the ventilation in TCC8 will be switched off, but in case of access to TCC8 the air will be flushed after a short cool-down period. In ECN3 the air will be re-circulated, with some fresh air in-take, to allow temperature control. The installation of the double wall is planned during LS1 and the renovation of the ventilation system itself is planned for the first half of 2015. For the 2014 run, some temporary measures are proposed to minimise the air flow from TCC8 to ECN3.

Further remaining work concerns the vacuum system for the blue decay tube which must be completed and the implementation of vacuum control for the beam and blue tube vacuum systems. Furthermore, the radio protection (RP) monitoring for the environment must be upgraded.

Parameter	Measured	Simulated
2 RMS at CEDAR: X [mm]	28	27
2 RMS at CEDAR: Y [mm]	15	15
Intrinsic angular spread: X' [mrad]	< 80	70
Intrinsic angular spread: Y' [mrad]	< 80	70
RMS at Big Fisc: X [mm]	12	12.6
RMS at Big Fisc: Y [mm]	14.6	15.1
RMS at MWPC: X [mm]	14.3	14.0
RMS at MWPC: Y [mm]	17.3	17.5
Rate normalised to nominal T10 flux	$3.6\ 10^9$	$4.5\ 10^9$

Table 2: Comparison between measured and simulated beam parameters

4 CEDAR / KTAG

Considerable progress has been made towards completing the optics and mechanical structure of the CEDAR-KTAG detector, including stabilising and monitoring the temperature of the KTAG enclosure and the implementation of an optical calibration system using an LED and optical fibres to illuminate the arrays of photomultipliers (PMTs). Thanks to the TR at CERN during November 2012, involving a prototype of the KTAG detector among others, considerable progress was made towards integrating the KTAG detector within the NA62 data acquisition system, including functionality of monitoring and data quality procedures. To complete the detector we will modify the optical components to enable illumination of all eight octants in the detector, each with 48 PMTs, compared with four active octants populated with 32 PMTs during the TR. The eight spots will be populated with the necessary frontend electronics and readout system; the prototype readout was tested during the TR, and further modifications are foreseen to the NINO boards. As part of this upgrade we are redesigning the optical stage for the 45-degree spherical mirrors to enable fine-tuning of the light spot to ensure maximum light acceptance by the PMTs. Finally, we will box in the region around the support cylinder between KTAG and CEDAR with thermally insulating panels to minimise heat exchange between the CEDAR gas and the environment. The purpose of the motor control system is to align the optical axis of the CEDAR with the beam axis, as well as controlling the diaphragm aperture. The motor system for (x,y) alignment and the diaphragm opening was tested in the TR, during which errors in the software were found and have since been corrected. The performance was 0.01 mm for y and the diaphragm and 0.05 mm for x. First results from the TR show that a time resolution of 100 ps or below and a kaon efficiency of about 90% is feasible. Further studies are under way to establish possible improvements and modifications. The detector will be completed and tested without beam in 2013 or early 2014.

4.1 KTAG Mechanics and Optics

KTAG (Fig. 13) consists of a rigid, lightweight structure in two halves that fits round the beam pipe and is cantilevered off a steel support cylinder rigidly fixed to the existing CEDAR detector. It is encased in a thermally insulating Faraday cage and thermal

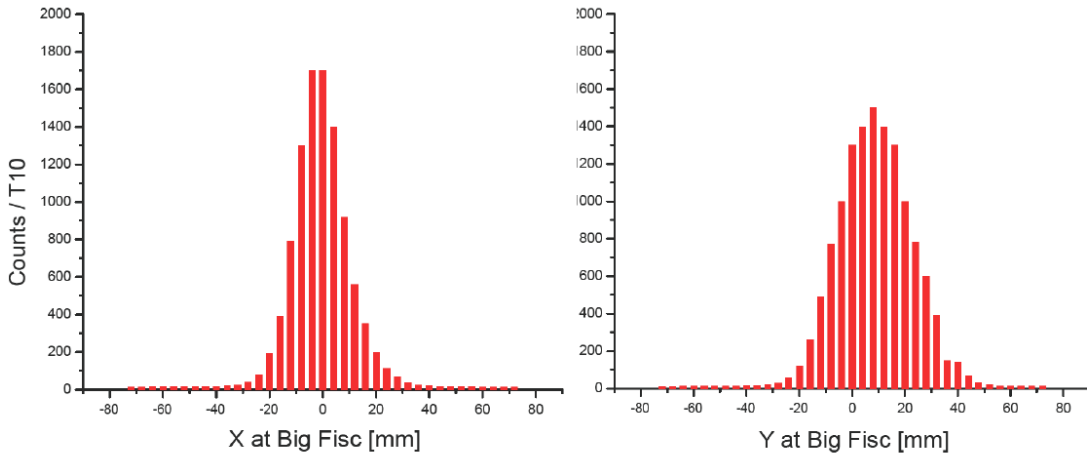

Figure 10: The beam profiles measured by the Big Fisc filament scanners

equilibrium is maintained by chilled water circulating through two stainless-steel loops. Monitoring of the electronics and optics is performed with a LED-Optical-fibre system. One of the technical concerns in the original design was the implementation of elliptical mirrors to reflect Cherenkov light radially outwards to the eight sets of PMTs. The concern here was the cost and time delay involved in the custom fabrication of ellipsoids with three different axes. A rather nice solution was achieved in Liverpool by the use of fused-silica spherical lenses covering the quartz exit windows of CEDAR in combination with 45-degree spherical mirrors to reflect the light. Simulation work in Birmingham enabled us to optimise the design to use commercially available lenses, while ultra-high reflectivity of the spherical mirrors was achieved by aluminising a set of glass lenses in CERN, thanks to the technical team led by Thomas Schneider.

The greatest technological challenge remained that of designing the lightguides to channel Cherenkov light onto the active surface of the PMTs. Simulation work was performed in Liverpool to optimise the conical geometry and layout in order to maximise the light reflected onto the PMTs. The design required a set of cones to be cut out of a spherical section of aluminium such that the conical axes intersect at the virtual source of light reflected from the spherical mirrors. This task was of such complexity that we kept it in house in order that we could rapidly make design modifications, should they prove necessary.

The achievable reflectivity of 78% for polished aluminium was not high enough to give the required optical performance and a better solution was found by gluing hollow cones of aluminised Mylar into the aluminium cones to achieve surface reflectivities of 90%

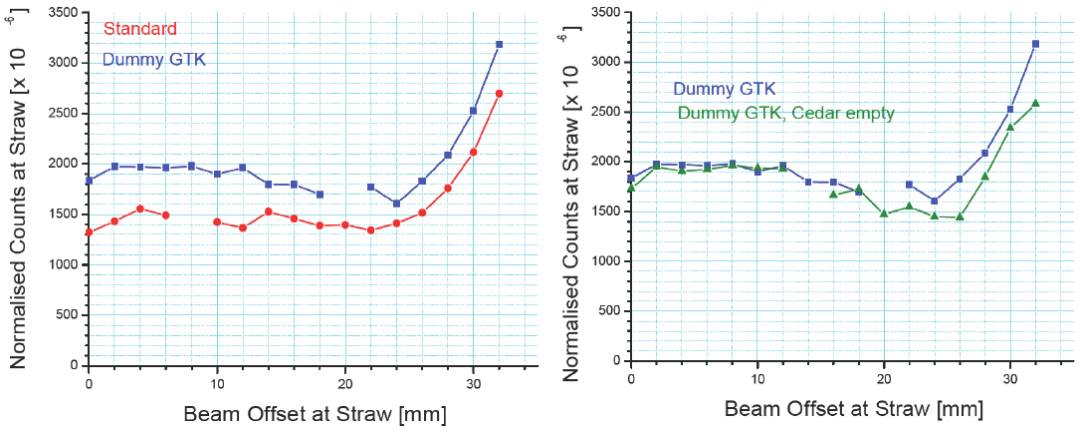

Figure 11: The increase of the rate in the straw closest to the beam when the beam is steered progressively towards that straw. The rates are measured in standard conditions (CEDAR full, no dummy GTK on beam) and with the CEDAR emptied or with the dummy GTK on the beam

across the wavelength spectrum. Once again, we profited from CERN technical expertise and used aluminised Mylar sheets developed by T. Schneider for the RICH detector.

In building the detector framework in Liverpool it was essential to ensure that it would fit precisely onto the CEDAR body in CERN. This was accomplished by commissioning two identical support cylinders off which the detector would be cantilevered. One cylinder was mounted onto a support frame in Liverpool, while the second was mounted onto the CEDAR at CERN.

Both halves of the detector framework were built to house the prototype electronics, cooling and monitoring equipment in order that the KTAG prototype would be mechanically stable when cantilevered off the support cylinder and fitted around the CERN beam pipe. During the TR of November 2012 the UK team equipped the KTAG prototype with four light boxes comprising 32 PMTs and readout electronics. Stainless steel cooling loops circulated chilled water around the enclosure to maintain a constant temperature and prevent heat leakage into the CEDAR gas, which would reduce kaon tagging-efficiency by broadening the Cherenkov ring.

A prototype LED-Optical-fibre system was implemented to illuminate the PMTs and enable monitoring of the electronics and any gradual deterioration in optical performance. The mechanics, optics and monitoring worked well and the way is now clear to transform the KTAG prototype into the final instrument for data taking.

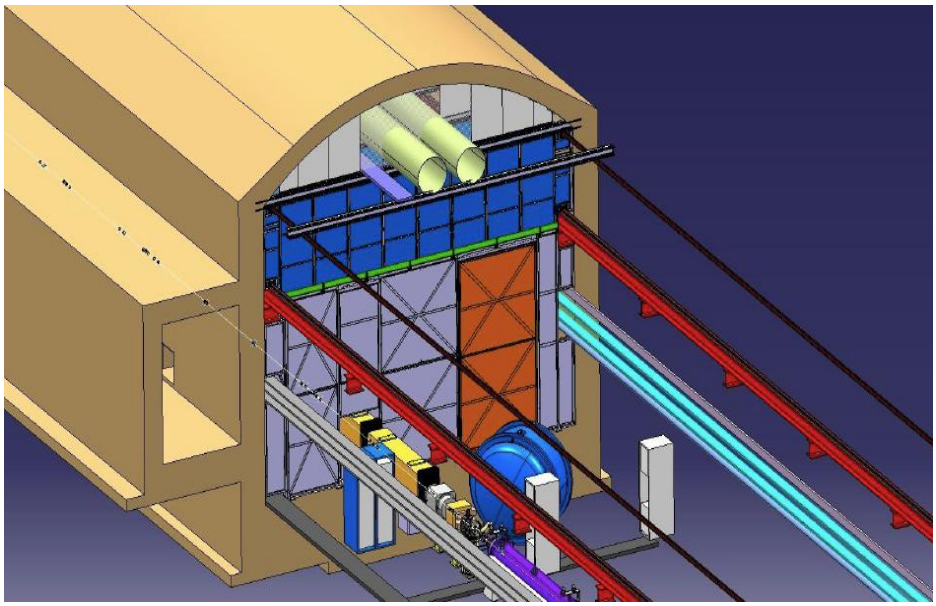

Figure 12: A view on the separation wall between the target region and the detector areas

The mechanical modifications necessary to complete the detector are relatively minor. Indeed, the structural integrity and outer Faraday enclosure have been proven during the TR. Now that a Flammable-Safety Derogation has been granted to maintain the original insulation within CEDAR, it remains to box in the region surrounding the KTAG support cylinder with panels of stainless steel thermally insulated with fire-retardant Rohacell 51S. The final design of KTAG includes provision for 64 PMTs per octant. However, with the currently foreseen K^+ beam intensity, simulation indicates that optimum performance will be achieved with only 48 channels per octant. This requires a change in the focal length of the lenses covering the quartz windows and in the radius of curvature of the 45-degree spherical mirrors, the implementation of which is currently in hand. Some difficulties were encountered in adjusting the reflected light spot to illuminate the arrays of PMTs and we are redesigning the optical stage on which the mirror is mounted to give greater flexibility. Further calibration work will be done with the LED-optical-fibre system to ensure the optimum operating conditions of the PMTs, and further calibration is necessary of the PT100s used to monitor the temperature of different regions of KTAG and CEDAR. All work will be completed during 2013.

4.2 Motor Control System

The alignment is carried out using an x-y stage positioned at the downstream end of the detector. The x-y position of the stage is measured using LVDTs. The same is true

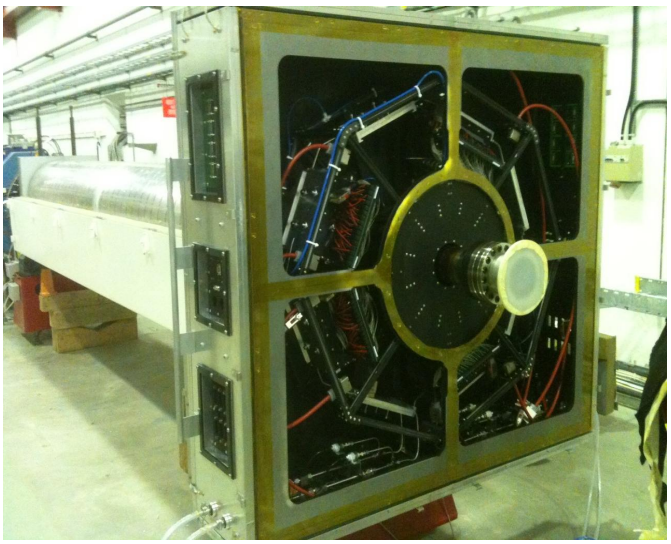

Figure 13: The KTAG prototype is shown supported off CEDAR on the beam line in the high intensity hall in CERN. Four of the eight octants are instrumented with the reduced number of 32 PMTs each. Cabling has yet to be attached to the patch panels on the side of the detector and 4 front doors complete the insulated Faraday cage within which the electronics, optics and cooling are mounted. The enclosure is flushed with dry nitrogen gas

for the diaphragm aperture. The system is controlled by a PLC that enables/disables a series of relays that energise the motors. The duration of energisation is determined using position feedback from the LVDTs. To ensure that the stages stay within their travel limits, end switches are used as emergency stops. The PLC, analogue module (for LVDT readings), digital module (for end switches) and relays are mounted in the server room above the cavern.

There is an additional switch for enabling/disabling the diaphragm end switches. This is in the form of a key switch and is needed so that when the radiator in the CEDAR is hydrogen the end switches can be disabled for safety reasons. The status of this switch feeds into the Detector Safety System (DSS). The hardware has been thoroughly tested and found to be in full working order. The user-interface for the motor control system is on the DCS and coded using PVSS, which provides an interface to the PLC. The software is designed so that the user should only need to input a position between the maximum and minimum limits for any of the coordinates. The system was tested in the 2012 TR, during which errors in the software were found and have since been corrected. The performance was 0.01 mm for y and the diaphragm and 0.05 mm for x and it will further improved.

4.3 Electronics and Readout

The frontend electronic and readout chain have been developed starting from that used for the RICH detector; however, a number of changes have been applied to make it more suitable for the KTAG. A custom socket was designed to allow for a PMT differential output to be used and low-power consumption; the socket connects each PMT R7400/U-

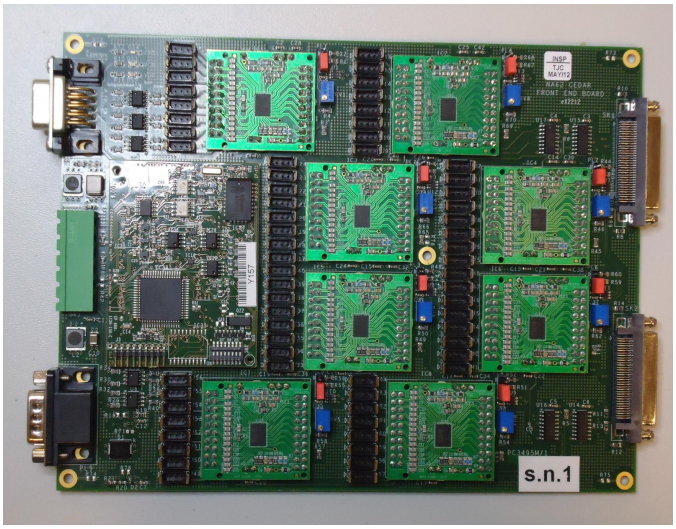

Figure 14: NINO custom board, prototype

03 to the high voltage (HV) and ground cables and to the NINO board via a differential signal cable. The NINO board is a custom board with eight NINO chips (ultra-fast amplifier/discriminator) for a maximum of 64 channel; the board among other things provides the power distribution for the NINO chips and a system to set and read the chip voltage threshold via DCS. A prototype of the custom NINO board was tested during the TR and generally gave good performances; a series of changes and improvements will be applied during 2013 and a revised version will be available towards the end of the year. A picture of the current prototype is shown in Fig. 14. The readout is then performed by a TEL62 board, which provides the trigger and the DAQ, hosting 4 daughter HPTDC boards (128 channels each).

4.4 Preliminary results from TR

Firstly the detector was aligned on the beam line using the positioning motors; a quasi-online monitoring system allowed to visualize the left-right and top-bottom asymmetries in the recorded light while compensation was performed moving the x,y motors in steps. The diaphragm was then set to 2 mm and a pressure scan was performed. Varying the vessel pressure, the detector is sensitive to different particle types in the beam, as it is visible in Fig. 15. The relative heights of the peaks is influenced by the kaon trigger purity used to record the data.

It can be seen that increasing the number of illuminated spots required, the pion and kaon peak separate. The position of the peaks has been found compatible with that observed with the same vessel in a test beam in 2011 (but with an older readout). Given that only four spots were equipped in 2012, the most stringent condition is to require four spot fired; it is anticipated that the likely working condition when eight spots will be operational in 2014 will be at least five spots but this condition will be firstly tested with another pressure scan at that time. An algorithm calculated the time of each kaon candidate in the event, considering that more than one kaon can be present in the readout time window. The difference between the reconstructed time and the average time is

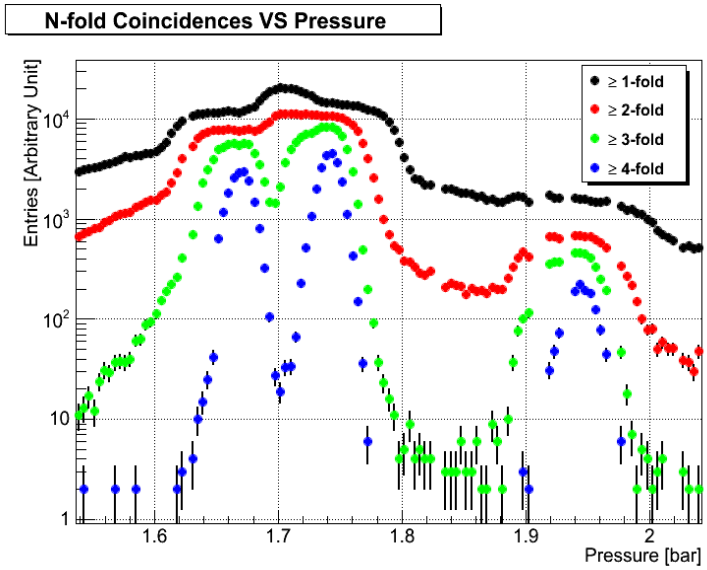

Figure 15: Varying the pressure the CEDAR is sensitive to pions, kaon, protons in the beam

visible in Fig. 16, where the original distribution has been corrected for the intrinsic time differences between various readout channels and by the slewing corrections. A time resolution of 280 ps (RMS) is obtained fitting a Gaussian to the peak. On the right side of the Gaussian peak a small excess of event out-of-time is visible: the origin of this small components of events is under investigation.

After applying a general selection, involving other detectors used in TR, to isolate a sample of kaon decays into two pions (see Sec. 14), charged and neutral, a distribution of the number of detected photons per kaon was produced (see Fig. 17). An average eight photons per kaon was measured (11.5 expected), and on the left side of the figure a residual contamination from non-kaon events of the order of 2% is visible, affecting bin 0 and bin 1. The same effect is visible in the distribution of octant in coincidence per event.

Considering eight detected photons per kaons, the overall time resolution reduces to about 100 ps. An overall kaon efficiency of 87% can be estimated considering at least three fired spots.

5 GigaTracKer (GTK)

The GigaTracKer (GTK) status report covers the main topics related to the detector construction. The following sections address, for each issue, the progresses made in 2012 and the road map towards the data taking in the Fall of 2014.

The following items are discussed: 1) Flip-chip bump-bonding; 2) Frontend micro channel cooling ; 3) ASIC development and GTK carrier ; 4) Mechanical integration; 5) Off-detector read-out electronics.

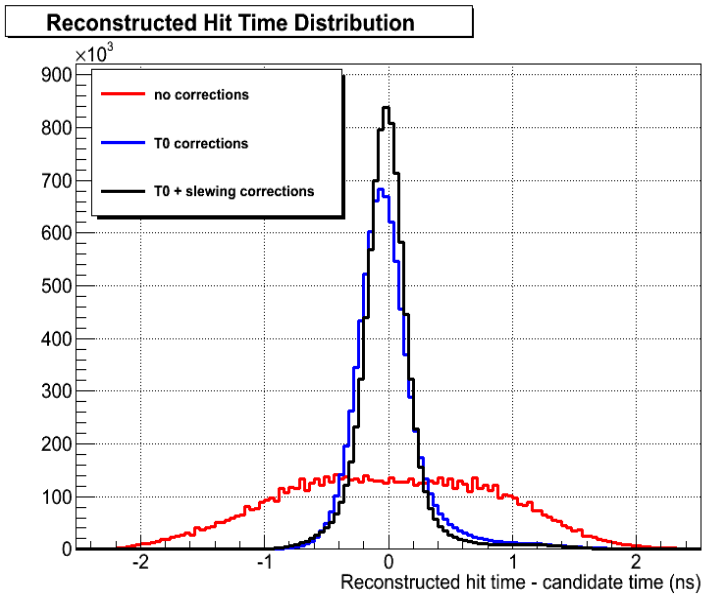

Figure 16: Hit time distribution; the RMS is 280 ps

5.1 Flip-chip bump-bonding

5.1.1 Activity in 2012

There are two main challenges related to the flip-chip bump-bonding. The most demanding is the bonding of the chips thinned down to 100 μm. The other challenge we have to meet is the relatively large bias voltage that will be applied to the sensor and the consequently necessary protection from discharge to be applied between sensor and chips. The chip thickness (100 μm) is required to minimize the material budget: particles interacting in the last GTK station (GTK3) can convey a large contribution to the lowest level trigger (L0). Furthermore, for the time measurement is required operating the GTK sensors at high over-depletion. This is obtained with a voltage above 400 V. A multi-guard ring structure is implemented in every sensor in order to ensure stable operation at this relatively high voltage.

In a synergy programme with the ALICE silicon tracker upgrade program, launched in 2012, the company IZM tested the complete step sequence: thinning of read-out chip wafers and bonding to the full-size sensors on dummy components. In this development the chip thickness had been reduced to 50 μm to cope with ALICE requests. The outcome of the development was not completely satisfactory. In fact, the thinning of the read-out chip and the bonding of the full-size sensor was indeed successful. Problems were encountered with the glass carrier removal. This is a delicate operation which is based on the induced mutation of the glue when treated with UV laser. However the operation delivers unwanted heat which tends to damage the deposited bumps. IZM could demonstrate that the glass carrier de-bonding on 50 μm chips can be done without damaging the chips. But, being the thermal budget for 50 μm-thick silicon chips being quite limited, it is recognized that, to avoid damages to the bumps, it is necessary to establish a procedure for the application of the laser power specifically tested for the

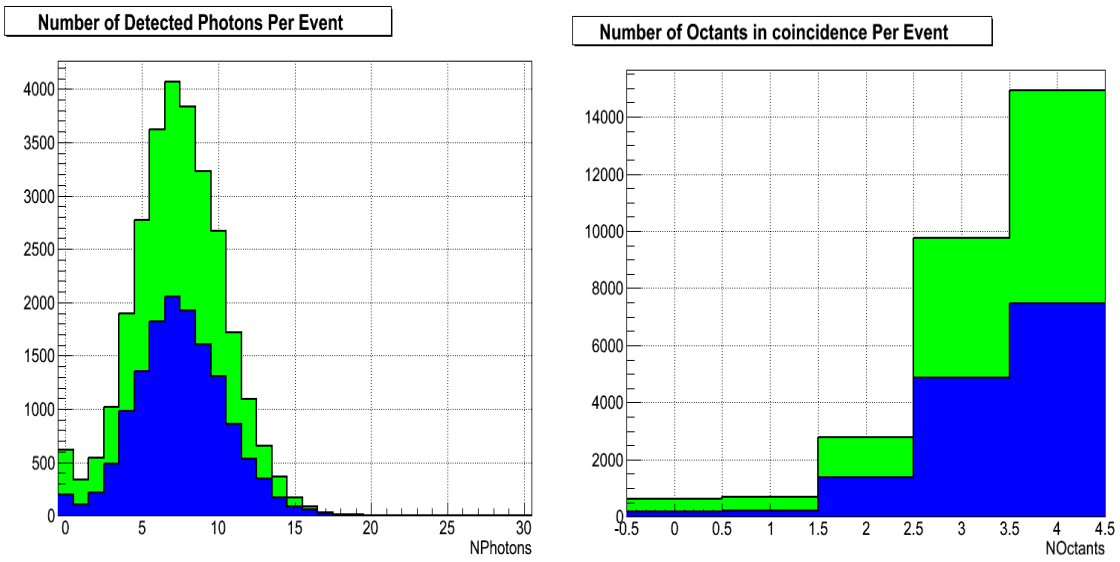

Figure 17: a) Number of detected photons per event. b) Number of octants in coincidence per event. The green curve is after selecting a pi0 signal in LKr. The blue curve is after selecting a signal for $K^+ \to \pi^+\pi^0$

dimensions of the assembly. Furthermore the chip area extends by 7.5 mm outside the sensor, increasing the difficulty of the operation. To summarize what we learned with respect to the two above mentioned challenges:

1. The glass carrier de-bonding procedure is still not functional and more tests are necessary.

2. An operating bias-voltage of 400 V has been achieved, while discharges start to occur at around 500 V. However, at 400 V the hit time resolution, as measured at the test beam, meets the specification ($\approx$ 170 ps).

5.1.2 Foreseen activity before the 2014 run

The *Invitation to Tender* for the production of the assemblies necessary for the run is being processed by the Contracts and IT Supplies section at CERN. Shortly the invitation will be sent to the two firms (IZM and VTT) which qualified at the Market Survey that we launched to classify firms according to our specifications. In our *Invitation to Tender*, we envisage two distinct phases: a) development; b) production. In the development phase, limited to six months, we ask the contractor to push further the identification of the procedure to assemble sensor and chips thinned down to 100 μm. We remark that several groups (ATLAS, ALICE, CMS) have investigated the thinning both with IZM

and VTT, and results look promising. On the other hand if the contractor will not be able to obtain in this period (six months) assemblies with such specifications, for the 2014 run the specification will be released by limiting the chip thinning to 150 or 200 μm. The production is quite limited in number and can be achieved in a few days.

5.2 Frontend micro channel cooling

5.2.1 The final performance tests of the baseline design

A ultra-thin micro channel silicon plate has been chosen as baseline cooling solution for GTK detector. Waiting for the final submission and testing of the GTK chip, the worst-case scenario for the thermal dissipation must be taken into account in the design of the cooling device. Therefore, although the desired nominal values should be significantly lower, during the qualification tests the power density has been assumed to be 5.4 W/cm^2 in the module's digital periphery and 0.65 W/cm^2 in the central sensitive area, for a total of 42.5 W. New silicon mock-heaters have been equipped with 20 resistive heaters, simulating the thermal behaviour of the digital and the analogue part of the 10 chips, thus allowing to power independently the region simulating the bump-bond connections to the sensor. These heaters provide a much more realistic temperature distribution, since they are made of the same material as the final readout chips.

The baseline design adopted for the thermal management device is based on 150 parallel cooling channels, each 200 μm wide and 70 μm deep separated by 200 μm walls. The channels cover the entire detector module surface and the cold liquid is distributed and recollected via two rectangular inlet and outlet manifolds, 1.6 mm wide and 0.28 mm deep. Fig. 18 schematically represents the cross section of the final cooling device. The amount of material crossed by beam particles depends on the position of the particle impact point with respect to the micro channel structure. The two cases are shown in Fig. 18: particles crossing the channel walls encounter (30+30+70) μm of silicon while the amount of material crossed by those particles passing through the channel is (30+30) μm of silicon summed to 70 μm of C_6F_{14}. The region where the detector module is glued is further selectively thinned by wet etching to a thickness of 30 μm above the channels. On the back side of the device, where the holes for the hydraulic connectors are opened, a second selective thinning is performed in order to minimize the material in the sensitive area.

Prototypes of this thermal management device have been produced and submitted to thorough testing in realistic operational conditions. Results obtained with the mock-up heater are summarized in Fig. 19, where we show an overall temperature difference map (bottom part of the figure) over the sensor and the profiles taken along three lines (upper part of the figure). The reference temperature ($\Delta T = 0$) is the inlet temperature of the fluid.

In the sensor area, the temperature variation over the whole surface of the detector module is smaller than 6°C. The temperature difference between the fluid and the warmest point on the detector surface is in the range 5-8°C. The devices can stand a pressure of 18 bars before failing in the manifold region and have been submitted to long term cycled pressure tests up to 12 bars without any observable deterioration. This provides a comfortable safety margin with respect to the 6 bars maximum pressure difference to the environment observed in operation, with a nominal 10 g/s flow rate of liquid C_6F_{14} at -20°C.

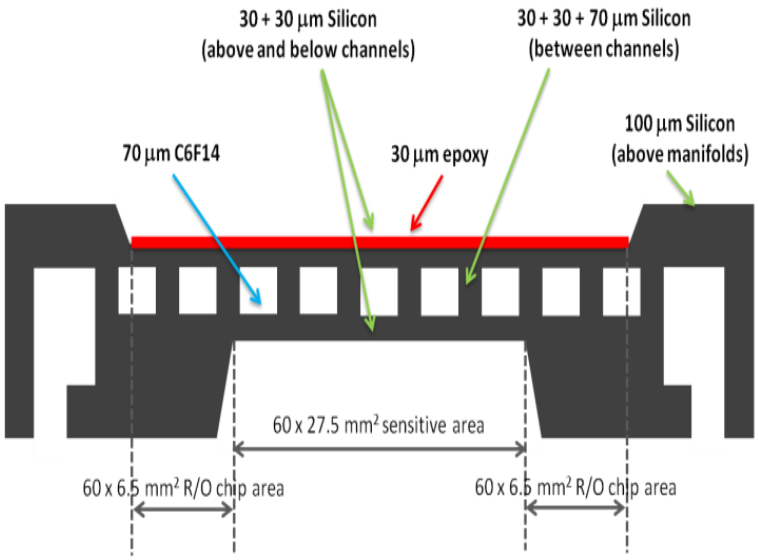

Figure 18: Cross section scheme of the GTK cooling device

5.2.2 Calculations and performance of an alternative frame design

In order to profit from the uneven distribution of thermal power in the GTK electronic for a further minimization of the material in the sensitive area, an alternative design is presently under evaluation. In this case, cooling channels are only placed in the digital chip region at the periphery of the detector module, and any additional material is removed from the sensitive area, where the power dissipation is eight times lower. Two narrow independent hydraulic circuits are etched in a silicon frame. As the cooling device is just outside the sensitive area, the requirement on the thickness can be relaxed, the channels can be deeper and a borosilicate cover can be envisaged. Preliminary results indicate that this option can provide a viable alternative to the baseline described above, depending on the final power distribution and on the thickness of the electronic chips, which directly relates to the thermal management performance.

After an iteration of the channel geometry, the measurements show that for a chip thickness of 200 μm the temperature spread of the pixel-sensor can be kept below 6°C. It also shows the excellent cooling performance of the micro channels that run under the high power digital part of the readout chips.

5.2.3 Soldered tube connectors

In order to improve vacuum tightness and stability, a connector for non-detachably joining pipes is desirable. Following the method described in [10], a steel tube equipped with a Swagelok ferrule was successfully soldered to the surface of a micro channels cooling

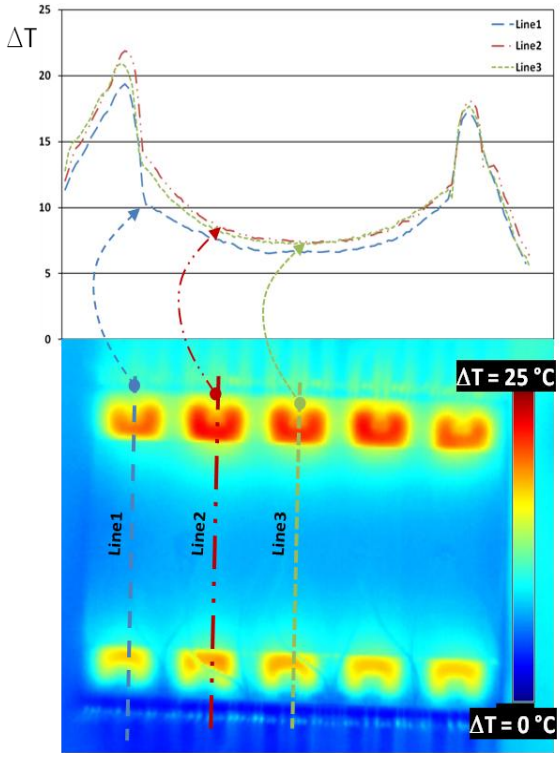

Figure 19: Temperature difference map as from measurements with the mock-up heater (bottom part); temperature difference profiles along three lines as indicated in the figure (upper part)

plate. This connection was later tested up to a pressure of 37 bars, which broke the 100 μm thick silicon. The solder connection was unharmed. The first thermo-hydraulic test was performed with CO_2 up to a pressure of 70 bars. Successive dedicated high pressure tests demonstrated a leak and structural resistance of the soldered connector up to pressures in excess of 250 bars. The soldered connections promise an excellent behavior in vacuum and in a radioactive environment. Further tests with the baseline cooling plate will follow.

5.2.4 Pre-production at IceMOS

The bid request for a pre-production run of Si-Si bonded devices produced to the final design and dimensions has been launched and the contract placed with IceMOS (UK). As this foundry works in 6" technology, it is possible to place on each wafer one baseline device and the two staves with hydraulic channels that can later be assembled into a frame device. Five of the six wafers ordered for this pre-production have been delivered in the last days (the last one being in its final processing phase at IceMOS). The devices will now be prepared for acceptance tests. In particular, one of the baseline devices will be immediately equipped with an available Si mock-up of the detector module (one 200 μm thick dummy sensor glued to ten 100 μm thick heater chips) and with soldered connectors for long term testing.

5.3 ASIC development and GTK carrier

The design work for several building blocks for the ASIC (TDC, read-out controller, configuration controller, pixel matrix, clock distribution) have been completed. Special care and time has been invested into the functional verification procedures. This is extremely important as the TDCpix ASIC is a large system on chip: 1800 frontend chains, 720 TDC (100 ps time bins) and a read-out processor with 4 x 3.2 Gbit/s. In addition to the 1800 frontend channels the chip contains functionality of components used in the LHC experiments equivalent to 22 HPTDC ASICs for the time tagging functionality, eight GOL ASICs for the data transmission. Furthermore the high speed and sensitive frontend is placed together with the high frequency readout processor and data transmission circuit on the same substrate with the requirement to maintain the timing resolution of 200 ps or better. An automatic procedure for the full chip physical assembly has been designed allowing timing and physical verification checks. The way the assembly process has been conducted allows immediate reassembly in case building blocks need to be changed. No manual interaction in the design is required. In the process of top level assembly optimization of the building blocks concerning the physical implementation is required. The top level functional and timing verification has been started. Submission verification checks have been started and are being optimized. Once the verification checks and the functional timing verifications have been completed the submission of the ASIC will follow. A detailed three-day design review for the building blocks and the design assembly was organized. The reviewers commented on the large amount of verification done, the detailed documentation available and on the advanced status of design and assembly. After the submission a stand-alone FPGA based test and qualifications system for single ASIC will be set up to allow lab, laser and beam tests.

The electro-mechanical interface has been defined with emphasis on the performance of the high-speed data transmission between the TDCpix ASIC and the electro-optical converters and a practical approach for the construction of the detector assembly. It was important that design choices on the TDCpix ASIC do not have negative influence on the hybrid or assembly construction or vice versa. The GTK carrier, which holds the GTK assembly (sensor, read-out chip and cooling), connects electrically the GTK assembly and acts as vacuum break, has been designed and is waiting for the final ASIC connections scheme. High speed simulations using AMI-IBIS models of the electro-optical converters have started to qualify the signal transmission performance between the ASIC and the electro-optical converters. Once the ASIC connections are fixed the next version of a GTK carrier prototype will be designed and constructed. This prototype will be used for integration studies and for ASIC system studies giving the possibility to power and operate 10 TDCpix chips. The chosen optical transceivers (miniPOD from AVAGO) will be tested on the GTK carrier prototype. For the calibration and timing critical reset signals (non DC balanced optical signals) two photo diodes (Ficer) have been qualified. For the low jitter clock signal transmission optical transmitters (OCP SRX24) have been qualified. Wire bonding tests have been done on the first mechanical GTK carrier prototype using a thermal mockup, which prove the feasibility of the connections between the GTK carrier and the TDCpix ASICs. The power supply system for the detector has been designed and together with the company CAEN a power supply module (3009K) was specified and designed. Tests on the 3009K low voltage power supply are in progress, they will continue after the reception of the prototype module which gave some problems. The optical and electrical connections in the cavern for LV,HV and the optical

connections have been designed and partially laid out.

5.4 Mechanical Integration

During 2012, the first mechanical prototype of the GTK1 and GTK2 mechanical structures have been produced. The structures are composed of two main elements: a) a frame where the GTK carrier is assembled and b) a vessel, where the frame can be inserted through one of the flanges. This design allows the use of the same frame for both GTK1-2 and GTK3 vessels. A vessel was installed during the TR to test both the compatibility of the interface with the beam pipe as well as the vacuum tightness.

During the last week of the TR a 380 μm slab of silicon was placed inside the vessel to measure the impact of a GTK station on the downstream detectors. The thickness, 380 μm of silicon, corresponds to the maximum amount of material of a GTK station. Due to this material crossed by beam particles, we expect mainly an increase of first-level trigger rate due to inelastic interactions with the silicon slab nuclei.

We remind that the GTK3 vessel is shared with the CHANTI. With the present mechanical design the GTK3 station is placed in the vessel using the very same frame as in GTK1 and GTK2, allowing to build all stations in the same way. During 2012, all mechanical interferences between the frame and the CHANTI setup were solved, and the final vessel production started.

5.5 Off-detector Electronics

The off-detector electronics will receive the data pushed by the TDCpix ASICs, save it on temporary buffers for the L0 trigger latency time, select the GTK data matching the L0 trigger request and send packets of events to the sub-detector PCs. These functions are performed by electronic modules dubbed GTK-RO.

Each on-detector ASIC is served by one GTK-RO module. The latter is actually made of two decked units: the mother board, which is a 6U VME card hosting the main functional blocks, and a daughter card featuring the interface to the TTC system and various timing functions required for the operation of the connected ASIC.

Starting March 2012 a series of validation tests on the GTK-RO prototypes has been carried out. Out of the first two boards manufactured one showed a faulty power section while, for the other board, all basic functions were found operational. A limitation found on the operating speed of one of the two DDR2 interfaces of the FPGA has prompted a time consuming survey of the key DDR2 signals and comparison with PCB simulation data. The information obtained was used to determine a set of FPGA configuration parameters which allows reliable operation of the interface at 240MHz.

A third prototype board was also manufactured and stuffed with the larger and faster FPGA foreseen for the production units. Since October 2012 and until now, the HDL source files determining the FPGA behavior have been refined and are currently being checked in hardware; this process has the goal of achieving timing closure of the FPGA design and testing the simultaneous operation of all the design modules which have been previously FPGA-tested individually. A microcontroller in the FPGA has been brought to operation; it has the task to measure variables such as the FPGA working temperature or the optical power level at the input of the transceivers. The prototype board that showed a manufacturing problem in the power section has been finally diagnosed through X-ray, reprocessed and will shortly be available for testing. By June 2012 the evaluation

of low jitter - high resolution programmable delay ICs and ancillary devices has been performed; these parts represent key components of a timing unit which will provide high precision timing signals to the on-detector ASICs. Throughout the second half of 2012 the benchmarking of the throughput of the links between a subdetector PC and multiple instances of the Ethernet MAC (implemented in the GTK-RO FPGA) has been successfully performed.

Concerning the hardware development, the activities foreseen from now until the 2014 run are:

- completing the debugging of the GTK-RO motherboard prototypes: as of now no need for a re-spin of the prototype PCB has emerged;
- signing off on the production of the full lot of GTK-RO modules (35 units);
- finalizing the schematic of the GTK-RO daughter cards and the high precision timing unit;
- learning how to operate the LTU ("Local Trigger Units") modules and the just recently delivered TTC-Ex modules;
- building and validating the daughter card / timing unit prototypes by means of the TTC signals generated by the LTU modules;
- install and test operation of the off-detector system in the field.

Concerning the software development, the activities foreseen from now until the 2014 run are:

- benchmarking with the actual GTK-RO prototypes and simulated GTK data the links towards the subdetector PC;
- implementing and benchmarking the "data producer" code running on the subdetector PC to pull data from the frontend cards and push it to the PC-farm;
- implementing the Ethernet-based slow control link between the subdetector PC and the GTK-RO cards connected to it;
- defining and implementing the communication protocol, possibly based on DIM, between the subdetector PC and the Detector Control System (DCS) of NA62.

6 CHANTI

The CHANTI detector aims at reducing the background induced by inelastic interactions of the beam with the last GTK station, GTK3. It detects the charged particles produced on GTK3 and emitted at relatively large angles w.r.t. the beam (while the rest of NA62 will be able to detect particles emitted at angles < 49 mrad) and is composed by six rectangular 300×300 mm^2 shaped hodoscopes with a 95×65 mm^2 hole in the center to leave room for the beam.

The first station is placed just 27 mm downstream off GTK3 while the other five are carefully placed to cover hermetically the angular region between 49 mrad and 1.15 rad.

Since the first station is very close to GTK3 the same vessel must host both GTK3 and the first 5 stations of the CHANTI.

Each CHANTI station is made in turn by scintillator bars of triangular section read by means of WLS fibers coupled to Hamamatsu Silicon Photomultipliers (SiPMs), for a total of 276 bars cut at three different lengths.

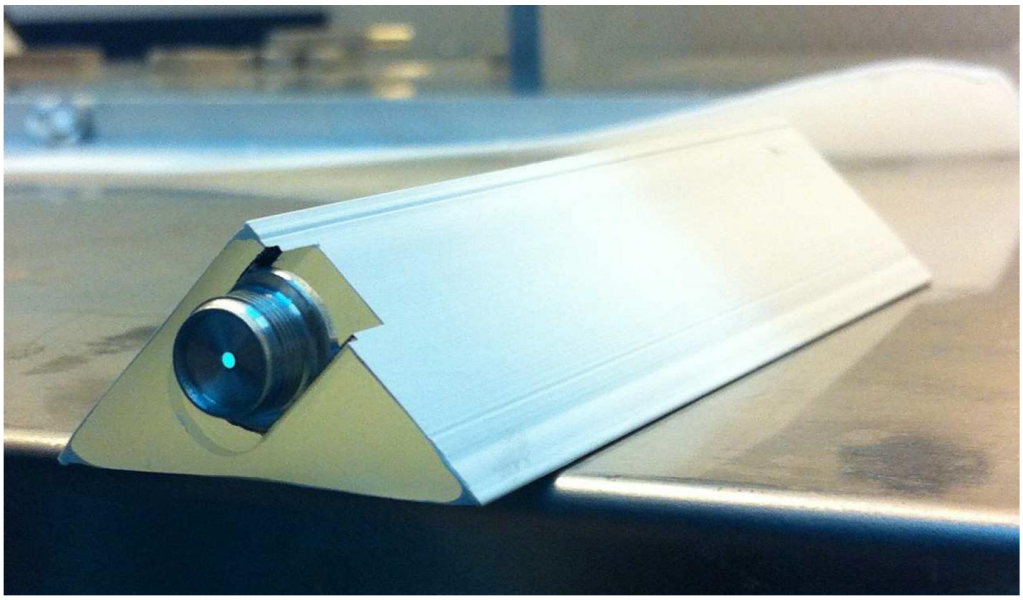

Figure 20: The triangular bar constituting the building block of the CHANTI detector. The WLS fiber with its custom connector is clearly visible

A considerable progress has been achieved during year 2012 on the CHANTI side. We will review it shortly in what follows.

6.1 Construction and tests

All of the construction and tests are performed in Naples, using dedicated tools developed by the INFN mechanical workshop. The construction phase starts by cutting the scintillator bars (produced at FNAL-NICADD facility) at three different lengths: 30 cm ("Long" bars), 11.75 cm ("Medium" bars) and 10.25 cm ("Short" bars). One side of each bar was machined to create the housing of the connector coupling the fiber to the SiPM (Fig. 20).

Fibers are mirrored at one side (opposite to SiPM), cut at the right length and glued to the connectors. Then, each fiber is inserted in the hole of the scintillator bar, kept vertical by a dedicated support. The free space between the fiber and the scintillator is filled by an optical glue (GE Silicones - Silicone Elastomer), injected slowly from the bottom to prevent air mixing. The glue was previously placed in a vacuum pump to extract the air in it that otherwise could create bubbles during the fixing.

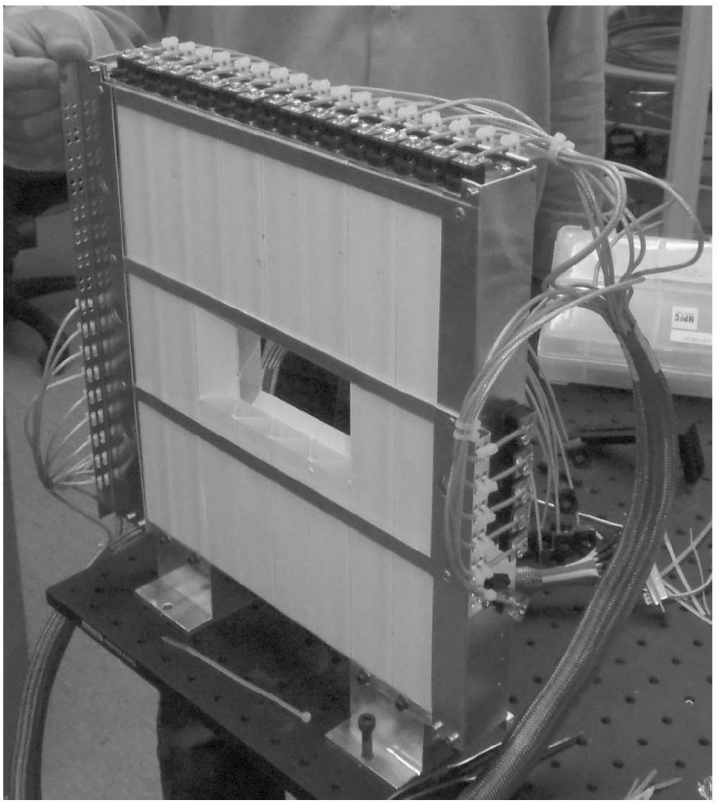

Figure 21: First CHANTI station with mechanical frame and full cabling

A structural glue (Epoxy 3MDP490) is used to fix the connector to the scintillator. The final aspect of the bar is shown in Fig. 20.

When the bars are ready, we perform a quality check and a characterization of each of them. We also characterize every SiPM.

After the tests, we used an alignment jig and the structural glue to assemble the first CHANTI station. At the end the station is housed in an aluminum frame and the SiPM are placed in their connectors. Since the SiPMs could be damaged by relatively small force applied to their pins, we designed a cabling solution based on a custom connector, a frame support and nylon bands. The first station, fully assembled, is shown in Fig. 21. Thanks to the adoption of appropriate design features and material choices, the overall outgassing of one station has been kept very low: it has been measured to be less than $3 \cdot 10^{-5}$ mbar l/s. All the construction procedure takes about 20 days for each station.

At present all of the 300 bars needed for the CHANTI have been fully assembled and one third of them have been also tested.

6.2 Frontend Electronics

The SiPMs by Hamamatsu used in the CHANTI are characterized by a typical operative reverse voltage of about 70V and produce fast (but small) signals with gains of order $7{\cdot}10^5$. They are not well suited to be used with common HV power supply, since their gain is quite sensitive to relatively small changes in the voltage bias which must be controlled at better than 0.1% level to achieve a satisfactory operating stability. Moreover since

Figure 22: The CHANTI frontend prototype board

the typical signal they produce is relatively small, it must be amplified before it can be discriminated and/or digitized. For the CHANTI we have thus designed a custom, all-in-one frontend board (see Fig. 22). It is both used to set the bias voltage of the SiPMs and to read their current. It also gives fast amplification to the signals before passing them in input to a comparator board (the LAV ToT board) which gives an LVDS output of duration equal to the time a signal is above a given threshold. The ToT board is actually able to give two LVDS outputs for each analogue input corresponding to different adjustable level thresholds. This feature can be used to correct for time-slewing effects. The main FEE board features are:

- voltage bias setting at 10 mV precision and very stable with temperature/time;
- current readout at nA precision;
- fast 25X amplification of analogue signal;
- temperature measurement via Pt100 probes;
- 32 channels in a VME 9U board;
- all settings and thresholds adjustable via CANOpen standard communication.

The prototype of the CHANTI frontend board has been used in the TR to operate the first station of the CHANTI.

6.3 CHANTI during the TR

The first station of the CHANTI has taken part in the TR in November 2012. The station was placed inside a small Al box and readout using the prototype frontend board. Since only 32 channels were available the 46 channels of the CHANTI have been readout

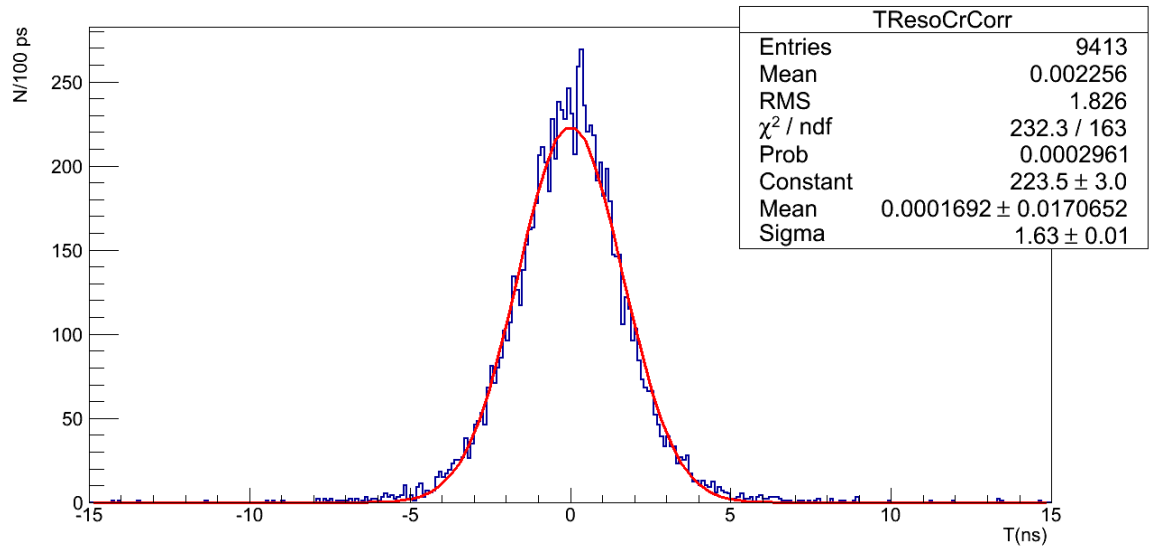

Figure 23: Distribution of the time difference among two fired bars in the TR, corrected both for time slewing and position effects. The fit to a Gaussian function is superimposed.

during the data taking in two overlapping groups of 32 channels each in two different configurations, by alternatively connecting two out of the three cabled feedthroughs. The CHANTI station has been placed outside the main vacuum and in proximity of the first LAV station (A1) and has been thus exposed only to the beam halo. Signals from the CHANTI FEE board were passed to the ToT board and then to a standard TEL62+TDCB readout. Actually, while only 32 physical channels were simultaneously connected, 64 TDC channels were acquired since the ToT board did provide two LVDS outputs corresponding to two different threshold levels. Both a stand-alone DCS and a stand-alone acquisition system have been developed in order to optimize the amount of data collected by the CHANTI, since these were clearly not correlated to the main trigger. However, mainly for DAQ checking purposes, usually during the night the CHANTI TEL62 was included into the standard common acquisition and data were successfully acquired in the common DAQ framework. The system was also operated successfully in vacuum, after connecting a pumping system to the Al box. Data have been acquired at different values for the thresholds and at different voltage bias and are being compared to a detailed G4 simulation of the bar response and of its signals developed in Naples. As a first and very important result obtained in the analysis of these data we show the time difference between two bars, corrected for both time slewing effects and position effects in Fig. 23. It is quite well fitted by a Gaussian with a $\sigma = 1.6$ ns thus indicating a single channel resolution of $\sigma = 1.6/\sqrt{2} = 1.1$ ns, perfectly in line with the detector requirements. The actual time resolution for a charged particle crossing one CHANTI station will of course be better since one expects two to four bars to be simultaneously fired on average, given the geometrical configuration of the detector.

7 Straw Tracker

The Straw Tracker is intended to measure the momentum and the direction of charged tracks originating from kaon decays. Recent progress involves:

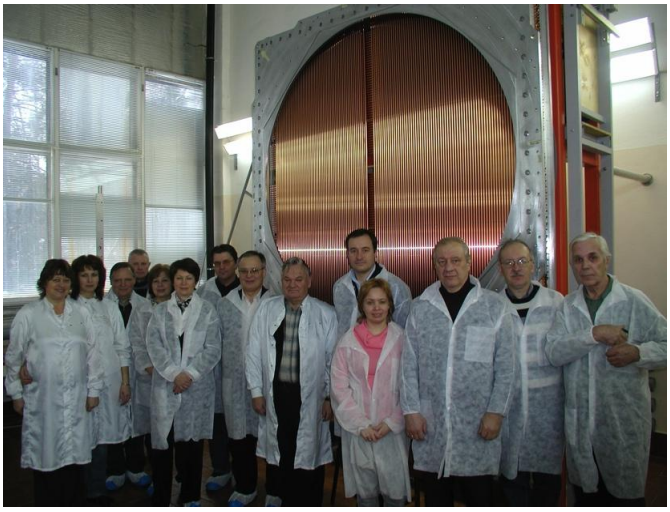

Figure 24: a) The straw insertion in the first module completed in Dubna (Module 3); b) Chamber one with one module containing the full set of straws connected to the vacuum tube just before the TR in 2012

- a total of more than 4 000 straws have been manufactured;
- procurement of all module frames and the rest of the mechanical components;
- technical transfer including a full set of assembly tooling to Dubna after validation at CERN;
- start-up of the module production in Dubna;
- the straw installation in the first production module in Dubna was completed in February 2013 (Fig. 24 a).

During the TR:

- Module 1 (1/2 chamber) was installed in the decay tank, together with its services and some frontend electronics (Fig. 24 b), 25 and 26);
- the Straws were operated under high voltage and rate measurements as a function of the beam distance to the nearest straw were performed (see Fig. 10);
- the readout board (SRB) is tested and the principles validated;
- the FPGA-based TDC have been integrated on the frontend board (cover) and tested successfully;

a) b)

Figure 25: a) The cabled part of the module in the TR. Four covers with the services connected are visible. b) One of the four services supports with the cable tray and one of the low voltage patch panels are visible in the centre

- the validation of the high and low voltage power supplies (Wiener MPOD) was performed;
- the validation of the low voltage patch panels and the design of the high voltage patch panels was completed.

The plans for the remainder of 2013 include:

- completion of the straw production (October 2013);
- design and production of the final cover;
- design of the full SRB (straw readout board) and firmware development;
- pre-production of the SRBs
- procurement of the remaining off-detector systems including the remaining gas racks, high and low voltage systems, patch panels and services;
- tuning of the detector performance will continue using the cosmic rays stand with the 64-straw prototype and the independent tracker based on four Micromegas modules.

Figure 26: The module manifolds ready to be equipped with the electronics covers. The webs with high voltage cables (red), signal connectors (white) and decoupling capacitors are visible

8 RICH

The RICH detector is needed to suppress the μ^+ contamination in the π^+ sample by a factor of at least 100 in the 15 to 35 GeV/c momentum range, to measure the pion crossing time with a resolution of about 100 ps and to produce the L0 trigger for a charged track. The detector will consist of a 17 m long tank, filled with neon gas at atmospheric pressure, with a mosaic of 20 spherical mirrors with 17 m focal length, placed at the downstream end, and about 2000 photomultipliers (PMTs) placed at the upstream end.

The order for the fabrication of the RICH vessel was submitted in November 2012. The RICH vessel is a vacuum proof tank, made of construction steel, subdivided into four cylindrical sections of decreasing diameter between 3.9 m (upstream end) and 3.2 m (downstream), together with a truncated cone shaped part for the connection with the upstream smaller diameter NA62 vacuum tank. The contract for the RICH vessel firmly establishes the delivery date by September 2013 and the installation in the NA62 cavern will take place in the fall of this year. The RICH exit window (end-cap) is a refurbished NA48 aluminum window; the entrance window is under fabrication. An aluminum beam pipe spanning the length of the RICH to keep undecayed beam particles in vacuum, is now under fabrication, with installation foreseen for the summer 2014.

The mirror mosaic (Fig. 27) is composed of 18 spherical mirrors of hexagonal shape (350 mm side) and two of semi-hexagonal shape to be located close to the beam pipe;

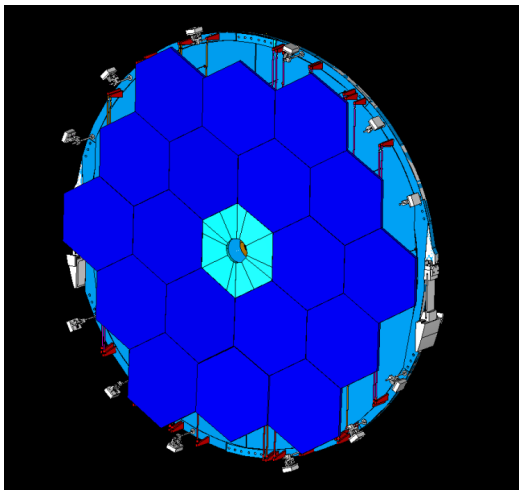

Figure 27: The mirror mosaic with the support panel (the two semi-hexagonal mirrors, close to the central hole, are not shown in this picture)

all the mirrors have already been manufactured, their optical quality has been tested and they are at CERN since summer 2011. The aluminization of the mirrors was delayed according to the RICH vessel delivery schedule and it is foreseen for spring 2013 at CERN; the coating process will take about three months.

An aluminum honeycomb panel will be placed in front of the downstream end-cap of the vessel to support the mirror mosaic; this panel, 50 mm thick and divided into two halves, was designed to be stiff enough for the 400 kg load of the mirror mosaic but at the same time as transparent as possible to photons to be seen from the downstream LKr calorimeter. The mirror alignment system is based on piezo-motor actuators connected to the mirrors by aluminum ribbons: all the piezo-motors (two for each mirror), with their encoders, have been already bought, a remote control system is under development.The mirror panel as well as the mirror support and actuating elements are been designed and prototyped at the moment. The resources assigned to this activities are been increased at the moment in order to meet the installation schedule in 2014.

Pure neon gas will be injected into the vessel after vacuum has been established inside; a system of gas purification and recirculation is also considered as a backup solution. The neon filling is cheduled at the end of the summer 2014.

The PMTs will be placed onto two disks 780 mm diameter each, closing off two cylinders protruding from a trumpet shaped flange connecting the largest section of the vessel with the upstream vacuum tank. Each disk will be made in two parts, both in aluminum: the inner part, 23 mm thick, separates neon from air by means of 12.7 mm wide, 1 mm thick quartz windows and collects the incoming light with a Winston cone; the outer part holds the PMTs. These disks have been machined in the mechanical workshop at the University of Florence in the fall 2011 and were brought at CERN for the gluing of the quartz windows and Mylar foils used to increase the reflectivity of each

Figure 28: a) Mylar foils ready to be glued on the Winston conces on the aluminium disk; b) winston cones with mylar foils glued on the aluminium disk (left row) and before gluing (right row)

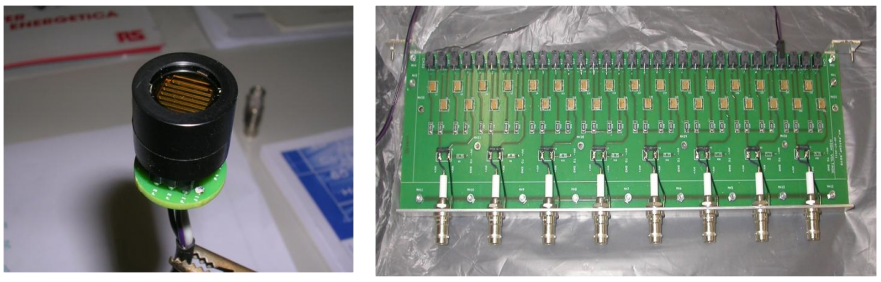

a) b)

Figure 29: a) A R7400U-03 photomultiplier with the new HV divider, without the final insulating case; b) One of the HV distribution boards: one HV channel (SHV connector at the bottom) feeds four PMTs (black connectors at the top); each board has 8 HV inputs and 32 HV outputs

Winston cone. This task took place in the summer 2012 with the help of technicians from Perugia and Protvino.

About 2150 Hamamatsu R7400-U03 PMTs have been bought, delivered and tested, including spares. PMT HV-dividers are custom made and will be delivered in spring 2013; all the required HV power supplies have been already purchased and are available.

HV distribution boards are in production and will be completed in spring 2013.

The PMTs readout electronics is also custom made: an executive design is under development and production will be completed by mid 2013; the readout electronics, based on the NINO ASIC, has been extensively checked in two test beam runs with a RICH prototype and a new version is needed only to provide the proper channel multiplicity required by the NA62 DAQ system.

We remind the reader that a full-length RICH prototype was built to demonstrate the feasibility of the RICH project and was tested in 2007 with 96 PMs and in 2009 with 414 PMs: the results of the 2007 and 2009 prototypes test beams have been published in [11] and [12], respectively.

The RICH schedule aims at the full installation to be completed and the detector to be commissioned before the NA62 physics run of the fall 2014.

9 Photon Veto

The principal achievements of the Photon Veto team in 2012 were in the design and construction and commissioning of the LAV system and small angle SAC detector, in particular we progress on:

- continued processing of lead-glass blocks for use in LAV stations A9, A10, and A11 (structural reinforcement, cleaning, characterization, and testing);
- Assembly and transport to CERN of A8 and A11;
- Production of final drawings for station A12, which is operated in air and thus of a different design from the other stations;
- Installation of the first 8 stations into the NA62 beamline;
- Vacuum-testing and measurement of outgassing for the stations installed;
- Mass production and testing of the LAV frontend electronics boards;
- Commissioning of the electronics for the first 3 stations;
- Development of level-zero trigger firmware for the LAV system;
- Installation of the SAC detector in the final position and commissionig during the TR.

9.1 Large-Angle Photon Veto

The LAV design is based on the reuse of the lead-glass blocks from the central part of the OPAL electromagnetic calorimeter barrel [13]. The blocks are made of SF57 lead glass and have an asymmetric, truncated square-pyramid shape. The front and rear faces of the blocks measure about 10×10 cm^2 and 11×11 cm^2, respectively; the blocks are 37 cm long. The modules are read out at the back side by Hamamatsu R2238 76-mm PMTs, coupled via 4-cm cylindrical light guides of SF57.

The LAV system consists of 12 stations. The diameter of the stations increases with distance from the target, as does the number of blocks in each, from 160 to 256, for a total of about 2500 blocks. Each station consists of four or five rings of blocks, with the blocks staggered in azimuth in successive rings. The total depth of a five-layer station is 27 radiation lengths. This structure guarantees high efficiency, hermeticity, and uniformity of response.

The first LAV station, A1, was constructed in 2009 and served as a prototype; three more of the upstream LAV stations, A2, A3, and A4, were built at LNF during 2010. In 2011, with the construction of A5, the series of stations of small diameter was completed. Stations A6 and A7, of intermediate diameter, were also constructed in 2011 [14]. Following the delivery of A7 to CERN in early 2012, stations A8 and A11 were constructed and delivered. A11 was the first station of large diameter to be completed and required the development of new technical solutions for aspects of the cabling and assembly. As of the end of 2012, nine of the 12 stations have been completed and delivered to CERN. So far during the construction of the LAV detectors, more than 1760 lead-glass blocks from the OPAL electromagnetic calorimeter have been processed (structural reinforced, cleaned, characterized, and tested), corresponding to $\sim 70\%$ of the total to be used in NA62.

Much progress has also been made on the mechanical design for stations A9 and A10. Since these two stations will be operated in the vicinity of the NA62 spectrometer magnet, the vacuum vessels in which they are housed must be constructed from high-quality, non-magnetic stainless steel. In 2012, significant effort was dedicated to identifying and

procuring an appropriate grade of non-magnetic stainless steel, and to developing techniques for its machining and welding. The contract for the fabrication of the vessels for A9 and A10 was awarded to Fantini SpA in mid-2012, with whom this work was carried out in collaboration. Construction of the A9 vessel has begun in September and for the A10 vessel shortly thereafter. These vessels are expected to be delivered to Frascati during the first half of 2013.

By the end of 2012, the basic design of the A12 station was completed. In particular, the arrangement of the blocks, the mechanical structure, and the basic cabling scheme were all finalized. The design of the A12 station, illustrated in Fig. 30, is different from that of the other 11 stations in many important aspects: it is operated in air rather than in vacuum, it is modular rather than monolithic because of its large size, and its installation into the closed space at the downstream end of the beamline will require a delicate insertion procedure. Also in 2012, stations A1 to A8 were installed in the

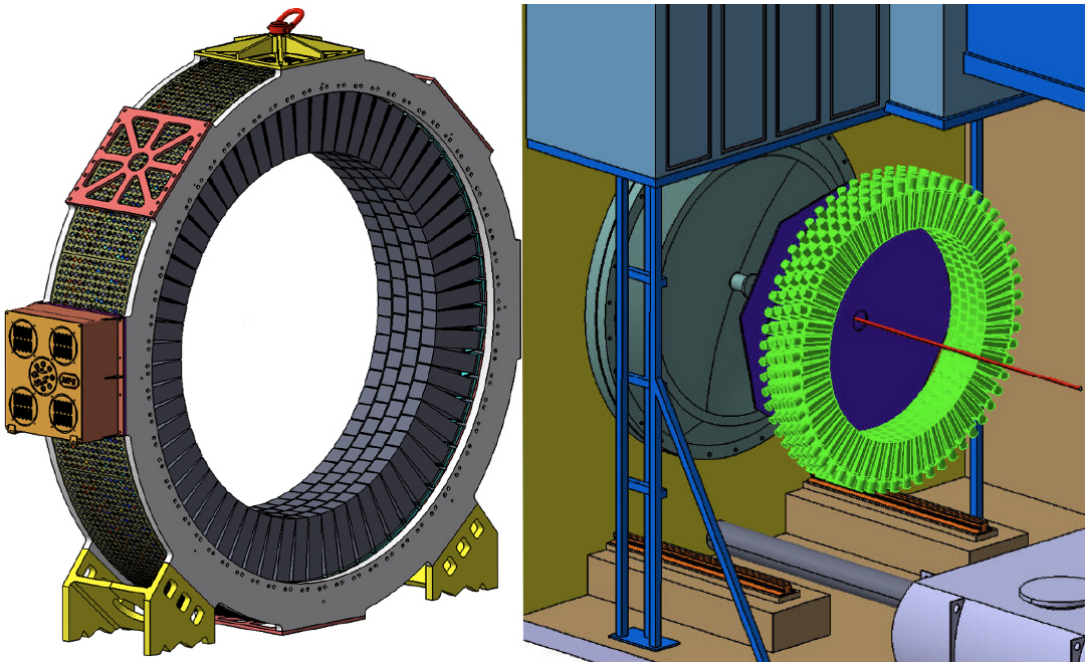

Figure 30: The LAV A12 station (left) and its insertion point in the NA62 experimental hall (right)

beamline and vacuum tested. The installation required a total of 26 person-weeks of continuous presence at CERN. In August, stations A1 to A3 were cabled, equipped with frontend electronics and digital readout cards, and read out with the NA62 data acquisition system in preparation for the first NA62 TR, which took place in November 2012.

The LAV system will mainly detect photons from kaon decays, as well as muons and pions in the beam halo. For each incoming particle, the veto detectors are expected to provide a time measurement with $\sim$1 ns resolution and an energy measurement of moderate precision (of order 10%). The system must be able to operate with thresholds of a few millivolts, well below the signal amplitude for minimum-ionizing particles (MIP) traversing the blocks, and maintain the detection efficiency as high as possible for muons and low energy photons.

Because of the intrinsic time resolution of the lead-glass blocks (<1ns) and the rise time of the Hamamatsu R2238 PMTs ($\sim$5 ns), the requirements on the precision of the

time measurement are not stringent. On the other hand, the amount of energy deposited in the LAV stations from photons from π^0 decays spans a very wide range, from about 100 MeV up to 30 GeV. Using the measured average photoelectron yield of 0.3 p.e./MeV and a nominal gain of $1 \cdot 10^6$ for the R2238 PMT, one expects a signal charge of ∼4.5 pC for a MIP, corresponding to a signal amplitude of ∼20 mV on a 50Ω load. At the upper end of the photon energy range, signals from 20 GeV showers can reach an amplitude of 10V. The readout chain for the LAV stations consists of two different types of boards

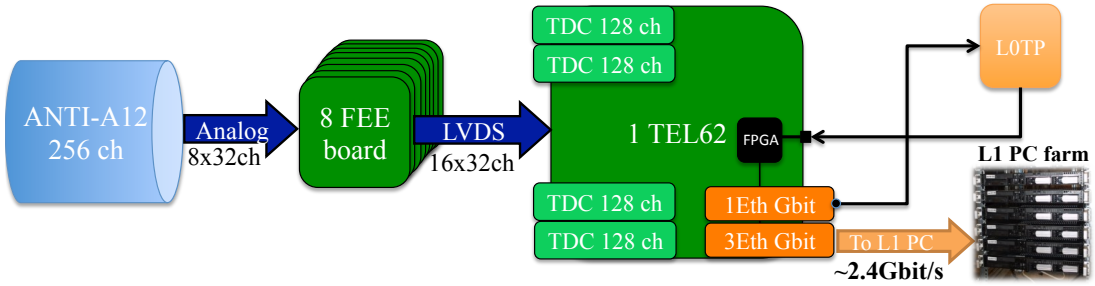

Figure 31: The LAV readout scheme. The A12 station has been used as example

(see Fig. 31): a dedicated frontend board (LAV-FEE) developed for the LAV detector, and a common digital readout board called TEL62, used by most of the NA62 detectors. The LAV-FEE splits the analogue signal from the PMT into two copies and converts each into a logical LVDS signal, using two comparators with independently adjustable thresholds. The duration of the LVDS pulses is equal to the time during which the analogue signal is above the programmed threshold. The LVDS logic signals are sent to the TEL62 readout board, in which a custom-designed TDC mezzanine converts each signal into digital leading and trailing times. The FPGAs on board of the TEL62 are used to correct raw hit times for slewing and to produce a level-zero (L0) trigger primitive, which is sent to the L0 trigger processor using a dedicated gigabit Ethernet interface. Upon receiving a L0 trigger request, the TEL62 sends its buffered data to the level-one (L1) PCs over three additional gigabit Ethernet interfaces. The whole LAV system has ∼ 2500 analogue input channels and ∼ 5000 digital output channels in total (one low and one high threshold digital output for each analogue input). The system is designed to sustain hit rates of up to 100 KHz per channel and to be able to transmit a data volume to the L1 PC farm of up to 2.4 Gbit/s for each station.

The basic idea is to exploit the time-over-threshold (ToT) technique to measure the signal charge over a broad interval. A custom 9U board designed by the LNF Servizio di Elettronica converts the analogue signals from the PMTs into logical LVDS signals of equivalent width, as described above. The LAV frontend board is implemented on a 9U VME standard layout with the J1 power connector only at the top of the backplane side. No VME bus line is connected to the board; only custom ±7.5 V power lines are used. At the bottom, the 32 analogue inputs are connected to the board using two DB37 connectors (see fig 32). The signal from each analogue input channel is discriminated at two different, programmable levels to produce two logical outputs. The resulting 64 LVDS outputs are available on two SCSI2 connectors placed on the front panel of the board for connection to the TDCs. Analogue sums of groups of 4 and 16 channels are provided on $8 + 2$ LEMO00 connectors for monitoring of the analogue signals. Communications with the board (e.g., for threshold programming) are managed by the CAN-Open protocol via two RJ-45 connectors. To simplify maintenance and reduce costs, the board has a modular

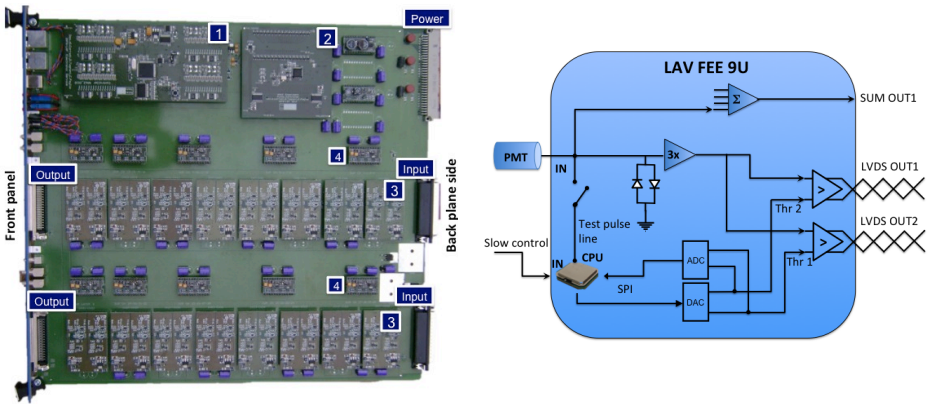

Figure 32: The LAV frontend board (left) and its block diagram (right)

structure. The 9U motherboard manages input, output, and power distribution while all other functions are implemented on mezzanines of four different types. A detailed description of each mezzanine can be found in [15].

The year 2012 was dedicated to the mass production and testing of the LAV-FEEs. One-hundred fully equipped boards have been produced, for a total of 1600 time-over-threshold mezzanines. Thirty boards were tested and characterized in advance of the NA62 TR in November 2012. The characterization and testing was performed at LNF using the automatic system described below. Of these, 26 were delivered to CERN and installed for the TR.

In order to test and characterize the 100 LAV-FEEs, an automated test stand was set up at LNF at the beginning of 2012. A pulse generator (Agilent 81110A) is used to generate test signals with a fixed rise time of 5 ns, a fall time of 16 ns, and variable amplitude. The signal is passively split into 32 copies and fed into the input DB37 connectors of a frontend board. The 64 LVDS outputs are connected to a VME commercial board (CAEN V1190B), which makes use of the same TDC ASIC as the actual TEL62 readout (HPTDC). The digital data from the TDCs are collected through a VME controller (CAEN V1718) and stored on a PC. The PC additionally sets the threshold values on the frontend boards via USB, and varies the amplitude of the signals from the pulse generator via GPIB. The procedure is fully automated; a complete test of a frontend board takes about 15 minutes.

Minimum threshold and time resolution measurements are performed for each board.To determine the minimum threshold, the amplitude of the input signal is varied over the range from 5 mV up to 20 mV. The threshold is set to the nominal value of 2 mV. This is the lowest value at which the noise rate is less than 100 Hz on each channel. The efficiency for each channel is measured as the number of pulses detected divided by the number delivered. An example of the result of this measurement is shown in Fig. 33, left. The minimum threshold is defined as the smallest value of the signal amplitude for which the efficiency is greater than 95%, as illustrated in the figure by the dashed red lines.

The time resolution is obtained by performing repeated measurements of the time difference between the leading and the trailing edges of a test input signal. The test signal is supplied by a pulse generator with a width of 30 ns and an RMS variation of less than 40 ps. The time resolution is then evaluated as the RMS of the distribution of the leading-trailing time difference. The distribution of the resulting values of the time resolution, for all channels on 26 boards, is shown in Fig. 33, right. Most channels have

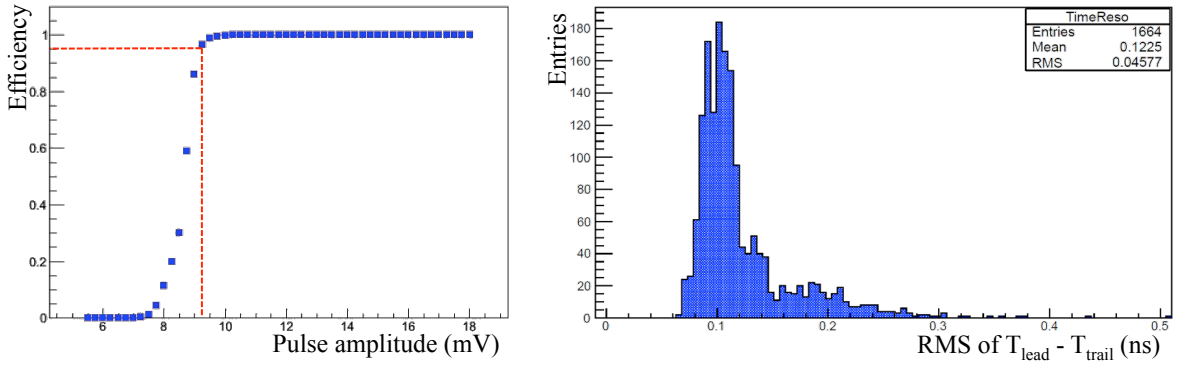

Figure 33: Left: threshold profile. Right: distribution of the RMS of repeated time measurements of a probe signal, performed with every channel. The probe signal has an amplitude of 100 mV and a fixed width of 30 ns to within 40 ps RMS

a time resolution on the order of 100 ps. The tail towards higher values is due to noisy channels that are still under study. If needed, the performance of these channels can be improved by replacing the noisy ToT mezzanines, thanks to the modular design of the frontend board.

For most of the NA62 detectors, the digital readout is based in the TEL62 board [16], which collects the data from TDC mezzanines and transfers them to the L1 PC farm via a gigabit Ethernet link upon receipt of a L0 trigger. Some of the detector subsystems, including the LAVs, must also generate the L0 trigger primitives. An L0 primitive is the value of the time at which some specific physics event occurred. To recognize this event and generate the primitive requires the development of detector-specific firmware for the FPGAs on board the TEL62s. In the case of the LAVs, the event which causes an L0 primitive to be generated is simply the receipt of a signal crossing both the low and high thresholds on the same block.

In 2012, the firmware to generate the L0 primitive for the LAVs was developed at LNF. The data stream for L0 primitive generation is independent of and parallel to that for the acquisition of LAV data. As a first step, events are distributed among different FIFOs, one for each low and high threshold channel. While the FIFOs are filled, a finite state machine searches for an event, i.e., a block with both thresholds crossed. Once the two hits are associated, the event time is determined, with slewing (time-walk) corrected according to the following formula:

$$t = t_{low} - \frac{(t_{high} - t_{low}) \cdot V_{low}}{V_{high} - V_{low}}$$

where V_{high} and V_{low} are the high and low threshold voltages and t_{high} and t_{low} are the respective crossing times. Events occurring within a specific time window (programmable up to ~ 25 ns) are then grouped together to form a cluster whose time is calculated as the average of single times. Finally, the time values of the clusters are sorted and delivered to the last firmware block to build the trigger primitives and send them to the experiment's L0 trigger processor.

The NA62 TR was carried out in November 2012. The LAV frontend boards were used to read out most of the detectors involved in the test. The 26 LAV-FEE boards available were installed in the readout chains of the CHOD (four boards), NHOD (one),

LAV (15), MUV (four), SAC (one), and CHANTI (one). The summed analogue outputs from the LAV-FEEs used to read out the CHOD and NHOD produced a L0 trigger signal for all detectors for the entire run.

During the TR, three complete LAV stations were powered up with the definitive HV systems and data were acquired with the final acquisition chain with muon and kaon beams. The entire readout chain was tested, with data recorded in the PC-farm. The data taken during the TR were used to verify that the channels and the associated electronics for LAV stations A1 to A3 were fully operational.

9.2 SAC and IRC

The small angle veto detectors covering photon angles down to zero degree with respect to kaon flight direction, SAC and IRC, are shashlyk type electromagnetic calorimeters. They are exposed to a very high rate of photons from kaon decays and (for the IRC) muons from pion and kaon decays.

The support table necessary for a precise positioning of the SAC detector inside the vacuum tube taking the non-decayed beam to the end of the experiment was designed and manufactured. It allows to align the detector horizontally (1 mm precision), vertically (1 mm precision) and to adjust the angle with respect to the beam axis with a precision better than 1 μrad. The latest is required in order to diminish the inefficiency due to photons flying along the WLS fibers. Both the mechanical components of the IRC detector and the SAC support table were transported to the NA62 experimental hall in the beginning of July, 2012. The SAC was installed in the 6 m long tube downstream of the experiment, cabled and tested. Before the TR the tube was evacuated, the covering plates of the detector were removed and both the high voltage and the readout system were reconnected in order to participate in the data taking.

The WLS fibers for the IRC detector were ordered and their delivery is expected within two months. Concerning the scintillator a study of the possible geometrical solutions and choices of tile manufacturer has been made. It was decided to procure 300 square tiles with side 150 mm and thickness of 1.5 mm and to perform the necessary cutting and drilling of the holes for the fibers afterwards. A sample of the chosen scintillator has been obtained from the producer and has been studied in order to verify its time properties since they are crucial for the performance of the detector at a very high particle rate. The type of the scintillator was found to be appropriate and the order will be placed in the present month. The machining of the scintillators and the assembly of the IRC detector will follow.

During the TR the SAC was operated and several issues were addressed. The detector was connected to two different readouts which were used in a standalone or in parallel mode:

- TDC readout: the signals from the detector were taken to the NA62 FEE board developed at LNF-INFN. The LVDS threshold suppressed output for each channel was then digitized by the TDC mezzanine mounted on a common TEL62 board. The data is processed by the common PC farm and the DAQ system of the experiment;

- ADC readout: the signals were connected to a 1 GS/s commercial flash analogue to digital converter manufactured by CAEN (V1751). The data was transmitted to a PC via an optical bridge and most of the time the readoutsystem was operated in a standalone mode, triggering on a minimal signal amplitude.

The main issues addressed at the TR were the ability of the SAC to detect signals from muons which was verified with the muon runs of the experiment. The operational plateau for a threshold of 10 mV was reached for a HV in the operational range of the installed PMTs. The rate without beam was measured with the TDC readout and was found to be at the order of mHz. The experience with the operation of the SAC with the flash ADC readout during the TR served as a baseline for defining the requirements of the RO system for the IRC detector. The data analysis is ongoing and the double pulse separation is under study.

Due to the high expected rate and the necessity to be able to distinguish between beam halo muons (occurring randomly) and low energy electron and positrons from photon conversions (in time with the event) an ADC readout is foreseen for the IRC. The necessary resources for the development of such a readout starting from zero for only four channels (eight, including the SAC) was found to be unreasonable and commercial solutions are under study for the moment. From the numerous available digitizers in the 500MS/s-1GS/s range (the minimal sampling rate is obtained by the signal rise-time, O(5ns)) five companies were identified to provide appropriate solutions and were contacted for further information with the goal of obtaining an evaluation board to perform tests of the digitization speed, possibility to handle external/internally generated triggers, precision of the event timestamping and customization possibility. The usual delivery time for such a board is two months after the ordering date. The decision will be taken based on the ability of integration of the board in the common NA62 DAQ system.

10 CHOD

The NA62 experimental apparatus comprises a fast scintillator system, called Charged Hodoscope (CHOD), to detect tracks with precise measurements of the arrival time and impact point, to provide a fast signal to drive the trigger and data aquisition (TDAQ) system and to suppress background signals when used in anti-coincidence.

According to the needs of the collaboration, the CHOD (which was a part of the NA48 setup) was refurbished in 2012 and extensively used during the dry run in July and the TR for multiple purposes (see subsections below for details):

- as a basic trigger element;
- as a tool to test HV system of the RICH and the new readout based on LAV-FEE and TEL62;
- as a part of the physics program during the TR.

These runs have demonstrated that the CHOD is in a very good shape. All channels worked properly providing high efficiency and good time resolution. The detector consists of two planes of 64 vertical (V-plane) and 64 horizontal (H-plane) plastic scintillators installed along the K12 beam line, upstream of the LKr calorimeter. The planes are centered in the beam direction with 121 cm external radius and 12.8 cm inner radius, suitable to contain the vacuum beam tube. The counters are made of BC408 plastic scintillator, 2 cm thick ($\sim$0.1 X_0), with lengths decreasing from 121 cm, closest to the beam pipe, to 60 cm and variable widths (6.5 cm for counters closest to beam line where the particle flux is higher and 9.9 cm for outer counters). Each plane consists of four quadrants made of 16 counters, providing a logic structure suitable for track triggering.

Plexiglass light guides with fishtail shape, 20 cm long, drive the scintillation light from one side of each counter to Philips photomultipliers (PM) of the type XP2262B (now produced by Photonis - ET Enterprises Ltd.).

The HV and readout systems were completely renewed. They are described in more detail below and in the RICH (HV) and Photon Veto (readout) sections of this report.

10.1 CHOD as the basic trigger element in 2012

CHOD was a crucial element of the trigger system during the TR. The CHOD trigger was made of analogue OR outputs from the LAV-FEE boards. The trigger logic was performed on NIM modules with 30 mV threshold. The modules were located near the detector and the trigger signal was transported to the L0 trigger processor. Before the L0 board the trigger signal was reshaped (700 mV amplitude, 20 ns length).

The trigger Q1 included at least one hit in both planes corresponding to the same quadrant:
$Q_1 = (QV_1 \& QH_1) \,||\, (QV_2 \& QH_2) \,||\, (QV_3 \& QH_3) \,||\, (QV_4 \& QH_4)$
where QV_i is the logical OR of all slabs in the quadrant V_i (i=1–4) and QH_i is the same for the horizontal plane.

10.2 CHOD as a tool to test HV system of the RICH and the new readout based on LAV-FEE and TEL62

The CHOD detector provided a unique opportunity to test the HV system that will be used for the RICH. In the TR, two SY1527 systems were used as power supplies for the CHOD PMs. Each SY1527 mainframe supplied the PMs of one hodoscope plane. Each quadrant (16 channels) was powered by a A1535S module. The module contains 24 channels, 16 of them were used. All channels were incorporated into the DCS and operated remotely.

The signals from PMs were readout by 4 LAV-FEE boards and one TEL62 board. LAV-FEE boards were also implemented into DCS and the thresholds were controlled remotely.

10.3 CHOD as a part of the physics program during the TR

The main goal of the physics program of the TR was to select the decay $K^+ \to \pi^+\pi^0$. CHOD with its good efficiency (channel map is shown in Fig. 34) and time resolution is an important part of this analysis.

To obtain a good time resolution of the CHOD, several time corrections were applied, i.e. ToT (time-over-threshold - time difference between trailing and leading time which is proportional to the amplitude) and T0 (absolute time values for all CHOD channels were aligned using the information from CEDAR that has a very good time resolution). After all corrections the time resolution for events with 2 hits in the CHOD was $\sim$300 ps (see Fig. 35).

In addition to the selection of the $K^+ \to \pi^+\pi^0$, CHOD was used to monitor beam properties during the TR (beam profile, hit multiplicity).

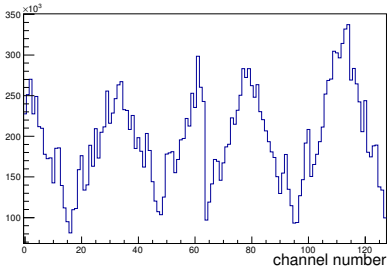

Figure 34: CHOD channel map

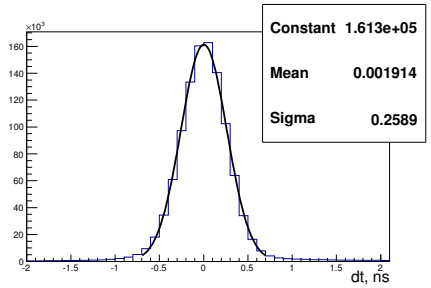

Figure 35: $T_{CHOD} - T_{Cedar}$ for events with 2 hits in the CHOD

11 LKr

11.1 LKr readout during the TR

In the previous report we described the preparatory work to be able to readout a subset of the LKr during the TR. An area of 64×64 cells around the center of the calorimeter has been equipped with the new power supplies, all the Fastbus branch connections where rerouted accordingly and all the CPD channels checked to be working. Another major achievement has been the integration of the new TTC-based trigger distribution system with the NA48 legacy one used by the actual LKr readout. This has been obtained with the TALK board, developed at CERN, which in 2012 acted both as L0 trigger processor and as LKr trigger interface. During the run, data were taken in various conditions of beam type and intensity. It must be noted that the 2012 data have been the first collected after 2008: as it is shown in Fig. 36, few malfunctioning areas in the calorimeter hitmap were noticed, and they were quickly understood and fixed. Calibration run were taken to have a good reference set for the collected data.

After the end of the run, we have started a campaign of checks, in order to identify possible problems and fix them well in advance of the 2014 physics run. For this, we move the available power supplies to configure pair of racks, reconfigure the Fastbus branch connection and collect both calibration and pedestal data. Symptomatic channels are then checked one by one with the oscilloscope to bypass possible problems in the CPD electronics. This campaign will be finished by April 2013.

11.2 New LKr readout

The work on the CREAM module at CAEN has progressed during 2012 with the complete definition of the hardware: board layout, type of FPGA, type of DDR3 memory, design of the analogue shaping daughter board, etc. In parallel the work on the firmware was first focused on the access to the DDR3 memory and later on the handling of the L0 trigger through the backplane and on the data transfer through the Ethernet link.

During the last days of the TR, a first pre-prototype was delivered at CERN and installed in the experimental area, connected to eight channels in the center of the calorimeter. The firmware was very basic: sampled data were collected in the memory and a snapshot of it was read every burst. No trigger handling was implemented. Physics and calibration data were collected. The noise was measured to be 2.5-3 ADC counts, well in agreement with the old readout. Fig. 37 and 38 show the distributions for the pedestals and a typical pulse shape. A very preliminary check of the time reso-

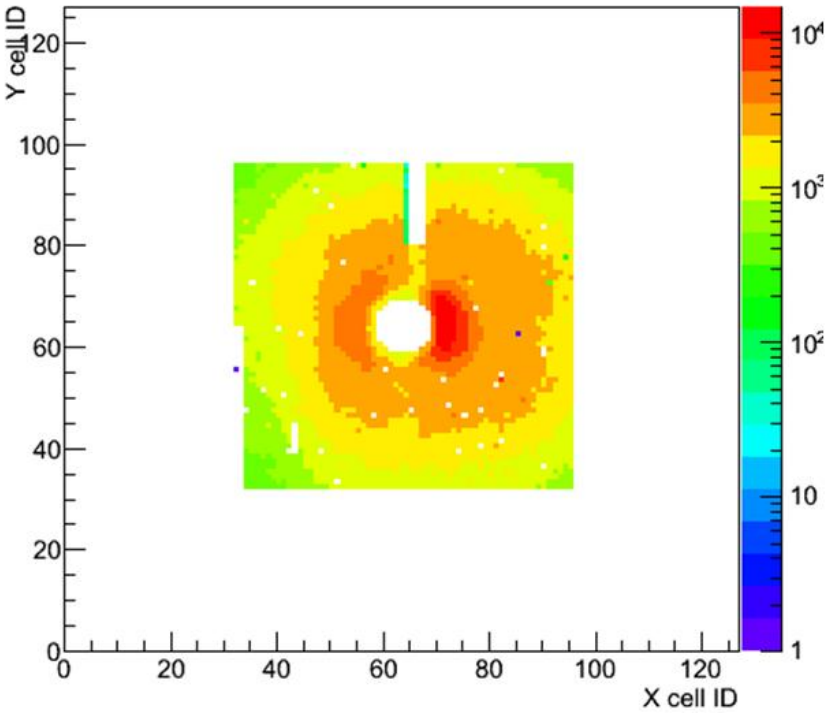

Figure 36: Cluster map of the LKr region read during the TR

lution using pair of channels is shown in Fig. 39. The current prototype being tested at CAEN is shown in Fig. 40.

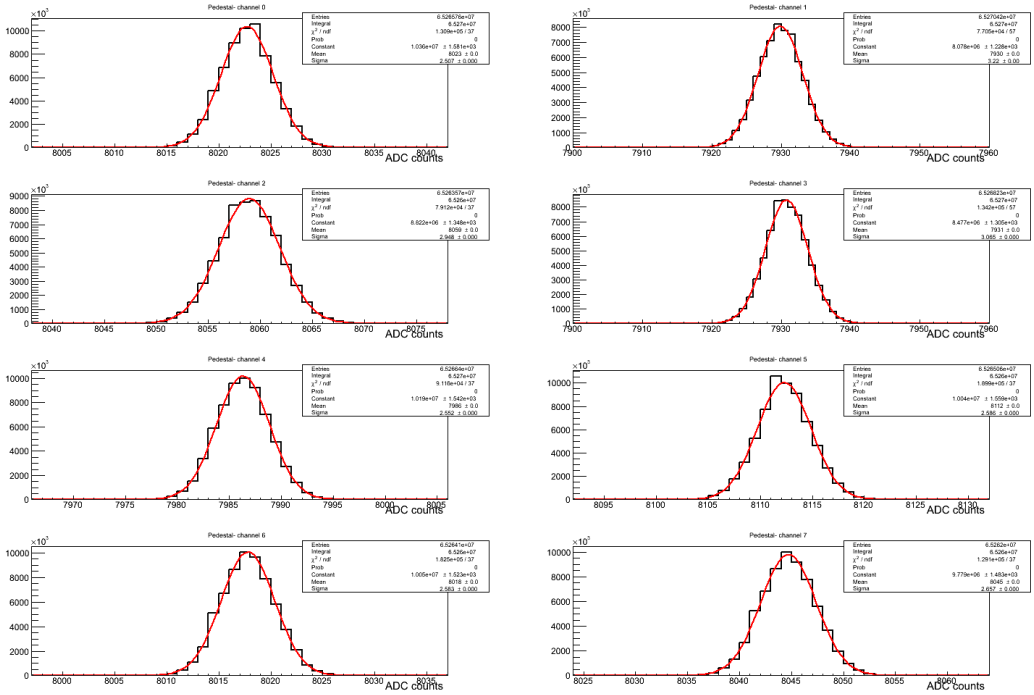

Figure 37: Pedestals distributions

CAEN will deliver two prototypes with a more complete version of the firmware by

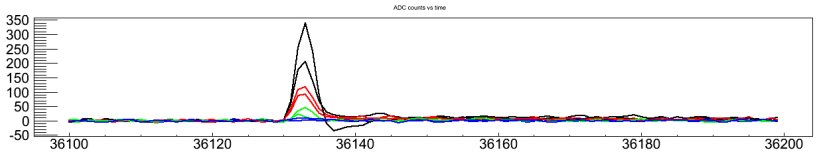

Figure 38: Shapes of typical digitized signals from the channels in a shower

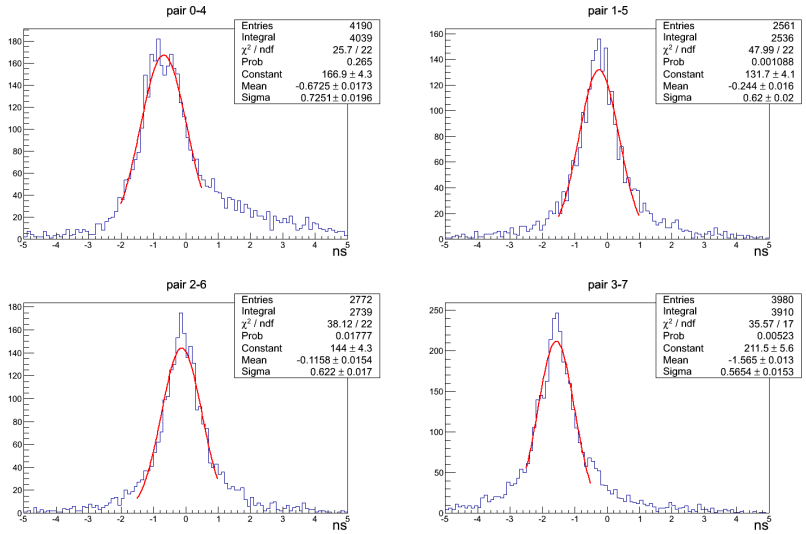

Figure 39: Preliminary time resolution distributions

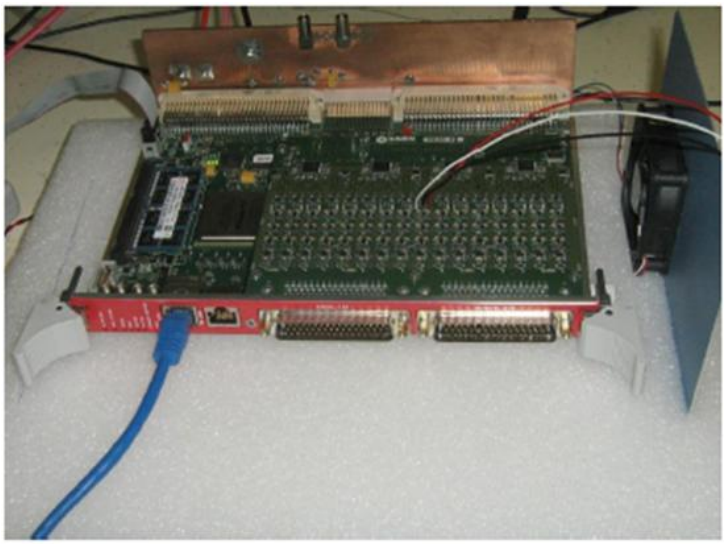

Figure 40: The CREAM prototype board

mid March. The setup for the validation of the boards has been setup at CERN. We plan to have a validation done by the beginning of June, in order to have a 10 board pre-production series by September, the first batch of delivery of 220 boards by the end of 2013 and the rest of the boards by March 2014.

At CERN, work on the clock distribution for the CREAM crates is progressing. The prototype of the crate backplane to distribute the clock has been tested, the final version of the PCB has been produced and it is being assembled. The design of the schematics and the firmware for the LKr TTC interface is finished, the layout is expected to be finished by mid March. Most of the critical components have been ordered.

The crates and the VME bridges for the final installation has been already bought. During 2013 we will buy the network switches and all the cables needed to start the setup of the infrastructure already this year. The installation and the commissioning of the CREAM modules in the experimental area will start as soon as the first batch of boards will be delivered and it will be completed by July 2014.

11.3 Cryogenics

An analysis of the status of the calorimeter cryogenics system and its control has been performed. A series of recommended actions have been listed. Priority will be given to the replacement of UPS for the control system, to setup a safe access to the cryogenics area on top of the calorimeter and to the replacement of the valve on the Argon cooler. Later, a spare LN_2 transfer line from the LN_2 dewars to ECN3 will be put in place.

12 Muon veto (MUV)

12.1 Introduction and Overview

The Muon Veto detector (MUV) is essential to veto kaon decays with muons in the final state. It consists of three independent subsequent modules, following the LKr and called MUV1, MUV2, and MUV3 in the order of their longitudinal position (Fig. 41). While MUV1 and MUV2 are iron scintillator sandwich calorimeters, the MUV3 detector consists of thick scintillator tiles for fast and efficient muon detection on the hardware trigger level.

The focus in 2012 was lying on the installation of the MUV2 and MUV3 detectors and the TR at the end of the year. In parallel, the scintillator production for the MUV1 was completed and many preparations for the final MUV1 construction were performed.

12.2 Progress on MUV1 Construction

The MUV1 module [17] is made of 25 iron and 24 scintillating layers with in total almost 1100 scintillating strips. The strips are read out with wavelength-shifting (WLS) fibres on both ends. For the production of the MUV1 scintillators, the Protvino group developed a new technique of melting polystyrene granulate together with the scintillating additives in vacuum at high temperature. This method allows the production of 270 cm long strips, needed for the MUV1, but avoids the usual time and manpower consuming procedure of extruding strips from large blocks. After several performance tests and improvements of

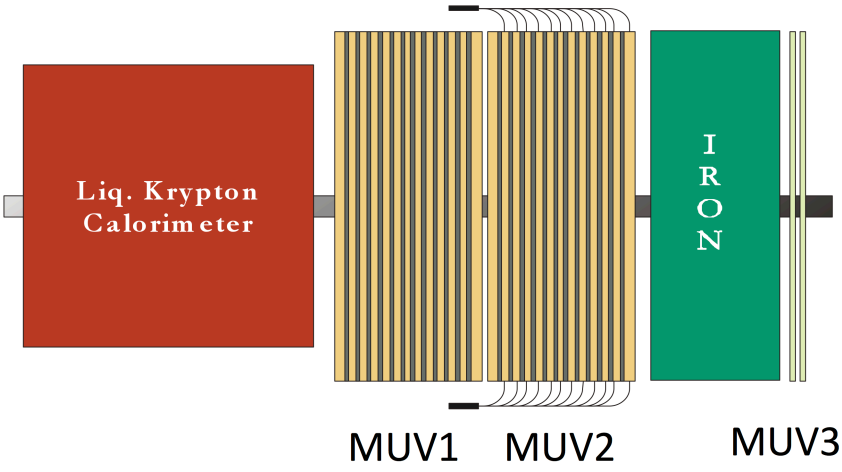

Figure 41: General set-up of the three muon veto detectors MUV1, MUV2, and MUV3. The beam entres from the left-hand side

the production procedure in 2011, the mass production was done and completed and all scintillator strips were shipped to Mainz during 2012[1].

In Mainz, the scintillators are further processed: Each strips obtains two grooves for the WLS fibres, the grooves are filled with optical glue, and the fibres are put in place into the glue. After measuring the performance in terms of light yield, each strip is wrapped in aluminized Mylar foil, being ready for the final assembly. Since these procedures have to be done for more than 1000 strips, machines and apparatuses were needed for automatization of each single step. Within the last year, all the necessary equipment was developed, built, and tested (see Fig. 42). The final MUV1 construction is also being done at the University of Mainz and is planned to be finished in 2013.

12.3 Installation of the MUV2 Detector

The main construction of the MUV2 detector, as a former NA48 hadron calorimeter (HAC) module, was left untouched for the operation in NA62. However, before the installation all PMTs of both NA48 HAC modules were shipped to Mainz for being tested and the HV settings being calibrated and recorded. Practically no degradation was seen with respect to the initial calibration in 1994. The best PMTs found in these tests were shipped back to CERN for the installation in the MUV2.

The actual installation of the MUV2 into the beam line took place in early Fall 2012 (see Fig. 43 (left)). After the installation, the PMTs were put in place and the detector was cabled up for HV and readout. It is worth noting, that the readout and HV systems, including the cable installation, are completely new and were not taken from NA48.

Since the MUV2 has similar requirements as the LAV detector, it was making use of the LAV-FEE electronics during the technical run. The outputs of the required 6 LAV-FEE boards were entering TDCB cards on a TEL62 board in exactly the same way as for the LAV detectors (see Fig. 44).

As the other MUV detectors, the MUV2 uses the same CAEN 4527 HV system as the LAV detectors. The HV modules had been ordered in 2011 and enough (three) were

[1]Since not all strips have been tested yet, there may be the need of a further small production. This would easily be possible, since the tools are still available at Protvino.

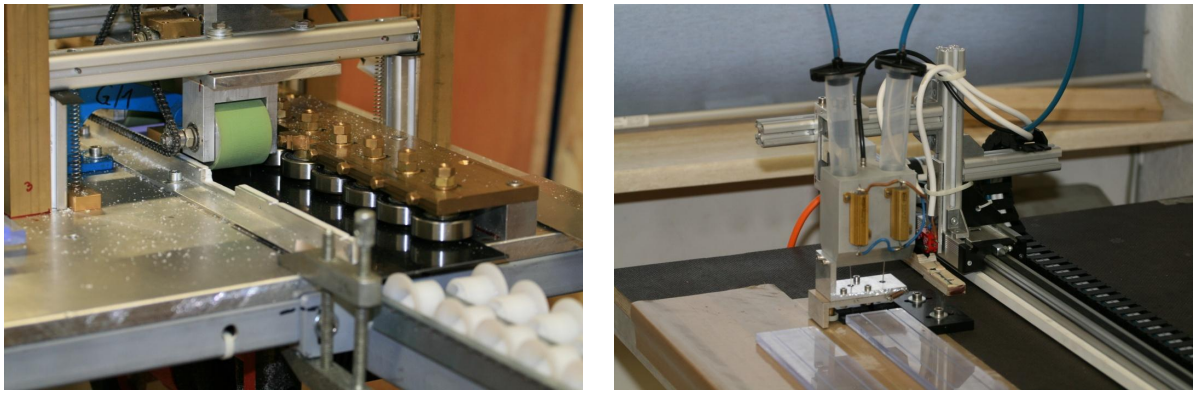

Figure 42: Left: Milling machine for the fibre grooves. The scintillator strips are pulled through from the front side; two saw blades (not seen) mill the grooves from the bottom. Cooling is done with pressurised air
Right: Machine to distribute optical glue into the scintillator grooves. Two syringes are moved forward with defined speed; the glue is pressed into the grooves by air pressure. Heating elements keep the glue at a defined temperature and viscosity during the process

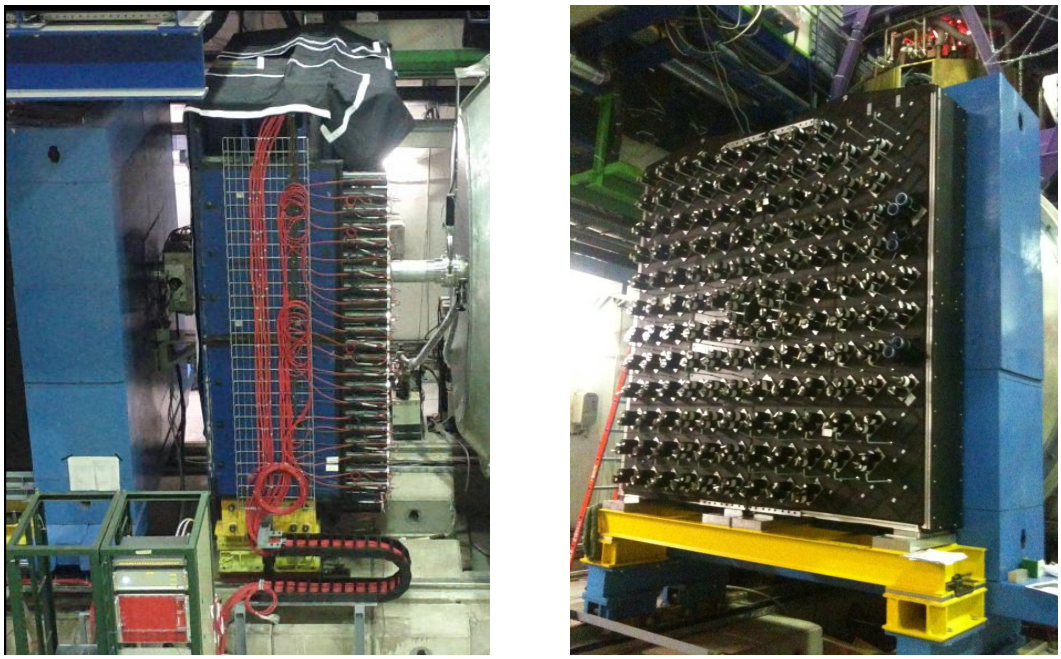

Figure 43: Left: MUV2 detector installed in the beamline with complete cabling; Right: MUV3 detector installed in the beamline, before the cabling

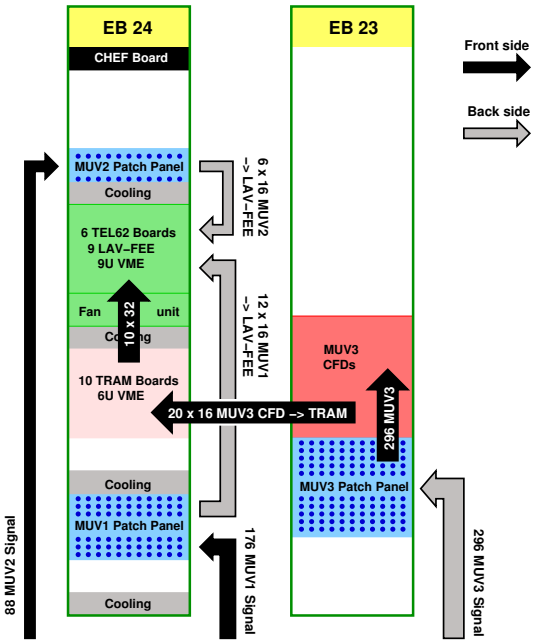

Figure 44: Cabling and data flow of the MUV readout. (No MUV1 cabling was done for the TR. Racks 23 and 24 are located in the NA62 Electronic Barrack.)

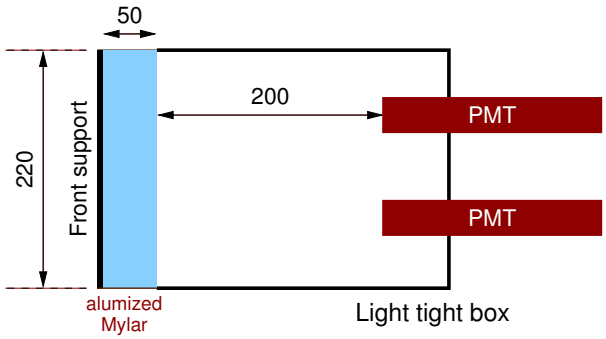

Figure 45: Sketch of one of 148 MUV3 cells

available for the 2012 technical run. To allow easy un-/recabling, the 32-channel CAEN HV connectors were split into single channels via patch panels.

12.4 Construction and Installation of the MUV3 Detector

The fast muon veto detector (MUV3), with sensitive area of 2640×2640 mm^2, was constructed in 2011 and the beginning of 2012 (Fig. 43 (right)). It consists of scintillating tiles of 220×220 mm^2 cross-section and 50 mm thickness, produced at IHEP (Protvino). Eight smaller tiles, each with one edge shaped as a 45° circular arc, are mounted around the beam pipe. On the back side, each tile is simultaneously read out by two PMTs (Fig. 45). The double-readout suppresses possible erroneous signals from Cherenkov radiation of particles crossing a PMT window. The whole detector was installed into the beam line in Summer 2012 and the readout and HV cabling was done in Fall 2012 before the technical run.

For the readout, the MUV3 reuses both the PMTs and the frontend electronics of the NA48 AKL detector. The PMTs were tested in Mainz together with the MUV2 PMTs and almost all were found to be in very good condition. Since only 270 PMTs were available, some cells were not equipped with PMTs. These cells are located on the Jura side and corners, where the rate during the TR was lowest. Additional PMTs will be obtained before the start of the NA62 run in 2014.

The MUV3 readout system consists of constant fraction discriminators (CFDs) of the NA48 AKL (see Fig. 44). One crate with 18 modules, each having 16 input channels, was available. Since the CFD outputs provide ECL signals, 10 new boards (TRAM boards, see Fig. 44), built in Mainz and housed in a 6U VME crate, are shifting the CFD signals from ECL via TTL to LVDS inputs for the TDCB boards. The final readout in 2014 will replace both the AKL CFDs and the TRAM boards with newly built CFD boards, based on the old design, but directly delivering LVDS signals. The production of these boards will take place in Mainz.

Also the MUV3 uses the CAEN 4527 HV system. The HV cards provide currents up to 1 mA per channel, just above the typical operating point of $\sim$ 0.8 mA at 1800 V for most PMT voltage dividers. However, 16 voltage dividers were of a different type, drawing $\sim$ 1.3 mA at 1800 V. Of these, 14 were replaced by lower current dividers, and 2 were connected to spare channels of the CHOD HV system. Furthermore, in contrast to its specifications, the HV system could not provide enough power for the operation of all 10 HV modules together. To overcome this limitation, a “power booster” was obtained

from CAEN and added to the crate (see also Sec. 12.5.2 below).

In contrast to MUV2, no patch panel is used for the MUV3 to split the output of the 32-channel HV modules to the single HV channels. Instead the single-channel cables were combined by crimping them into the 32-channel connectors, which led to several problems with bad HV connections during the installation. During the TR, however, no connectivity problems appeared.

12.5 MUV2 and MUV3 in the Technical Run

12.5.1 MUV2 Performance

Due to the late detector installation and the late delivery of HV modules, the MUV2 detector (as well as MUV3, too) could only be cabled shortly before the start of the technical run and tested and calibrated partially only during the run.

After calibration, most of the MUV2 PMTs were operated at high voltages close to the voltages determined by the calibration in Mainz. Out of the total of 88 channels, six PMTs were noisy, most likely due to light leaks which occurred during the dismantling and refurbishment of parts of the detector surface[2]. This is supported by the fact, that most of the noisy channels were in the top vertical row of scintillator strips, a place where possible problems with light leaks were expected. Due to the non-accessibility of the detector front face before and during the run, no further investigations could be performed. The six noisy channels therefore were disabled in the run and will be investigated during the shutdown period.

An additional problem occurred in the readout: the time differences between the rising- and falling edges of the MUV2 PMT pulses[3], were often larger than 75 ns. As this was the maximum possible time difference allowed in the TEL62 firmware, about 50 % of the pulses were stored without either the leading or the trailing edge and were therefore useless for the analysis. The situation could only partially be improved by lowering the PMT HVs and thereby the time-over-threshold (ToT).

Despite these problems, many good runs and events were recorded. For a hadron beam, Fig. 46 (left) shows the sum of all ToT values of crossing strips with both strips having both leading and trailing edge stored. Clearly be seen is the increase in intensity towards the beam pipe[4]. Also, the six disabled strips are clearly visible.

12.5.2 MUV3 Performance

Due to the late installation and the late delivery of HV modules, also the MUV3 detector could only be cabled shortly before the start of the technical run.

At the beginning of the run, in total 14 noisy CFD channels were found and disconnected. Together with one bad SHV connector, the missing PMTs, and faulty CFD channels (see above) a total of 38 cells (from 148) did not have both PMTs in operation. Due to the necessary installation of the CAEN power booster (see above) and its breakdown after 9 days, a useful run time was only possible for about one week of hadron beam.

[2]In NA48, the HAC was operated inside a hood covered by black cloth. Due to the available space and the new cabling, this hood is not used in NA62 any more.

[3]The shaped signals were provided as outputs from the LAV-FEE boards (see above), which worked as expected.

[4]The red spot, however, is due to noise.

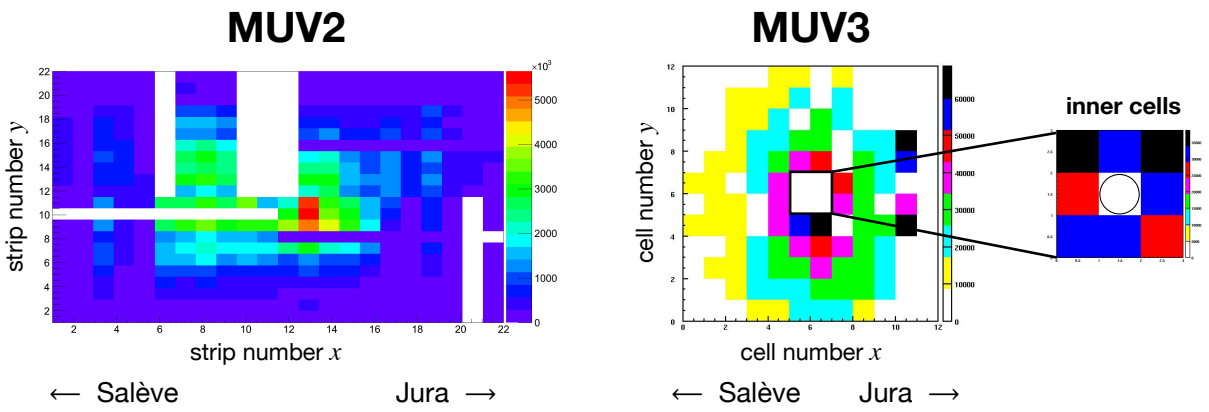

Figure 46: Left: MUV2 hit map of events with crossing vertical and horizontal channels. The histogram entries represent the sum of all time-over-threshold values. Right: MUV3 hit map of events with both PMTs of a cell firing within 9.8 ns

A hit map of the MUV3 is shown in Fig. 46 (right). A good hit is defined, if both PMTs see a signal within 9.8 ns. As for the MUV2, the rise in intensity towards the beam pipe is clearly visible.

The MUV3 time resolution can be measured using the time difference $\Delta t = t_1 - t_2$ between the two PMTs of one cell. Using the standard deviation of all measured time differences, resolutions were $\sigma_{\Delta t} \sim 0.5-0.6$ ns. Fitting the peak region of one distribution with a Gaussian gave $\sigma_{\Delta t} \approx 0.35$ ns. Both values are better than the required time resolution for the L0 trigger.

When measuring the time resolution it was discovered, that many channels see a double-peak structure in Δt with both peaks about 1–2 ns apart. Investigations showed that, most probably, a flip-flop of the old AKL CFD electronics is responsible for this feature. This will be taken into account when rebuilding the CFDs for the NA62 experiment.

12.5.3 MUV Conclusions from the TR

In summary, the following conclusions can be drawn from the technical run:

- Despite several noisy and non-equipped channels, both detectors have in general performed well in the TR. In particular the measured MUV3 time resolution of about 0.5 ns is well within the requirements.
- The HV system had some problems during the setup (fragile connectors) and running (operation only possible with an additional power booster). For the latter, a good and stable solution still needs to be found for the final running in 2014.
- The readout of the MUV2 via LAV-FEE boards worked fine, but suffered from the inability of the TEL62 boards to store time differences of more than 75 ns. This problem needs to be solved before the start of NA62 end of 2014 by either modification of the TEL62 or the use of different electronics for the MUV1 and MUV2 readout[5].

[5]The latter is anyway investigated, since the LAV-FEE boards are in principle over-equipped for the MUV1 and MUV2 needs.

- The MUV3 readout with the old AKL CFDs in combination with the TRAM level shifter boards have worked well, except for oscillations in the time measurements in some channels. These oscillations have been traced back to the CFD boards and will be taken into account in the new production of CFD boards for the final set-up.

13 Trigger and Data Acquisition

During last year the activity in the TDAQ group focused towards the finalization of prototype systems for the sub-detectors to be tested during the test runs of 2012. Two coordinated runs were foreseen and carried out: a *dry run* during the summer without beam, specifically intended for TDAQ installation and testing, and the actual TR with beam in fall, in which sub-detector data was collected.

While TDAQ progress is still behind the original schedule mostly due to manpower issues, the programming of the runs, had a highly beneficial effect resulting in a significant step forward in the implementation and understanding of many important issues.

The goal of the summer dry run was to install and inter-operate for the first time NA62 TDAQ equipment in ECN3. The focus was to test the sub-detectors sharing the most advanced readout system, namely the common TEL62/TDCB-based (Fig. 47), with other sub-detectors hoping to join later with partial readout prototypes.

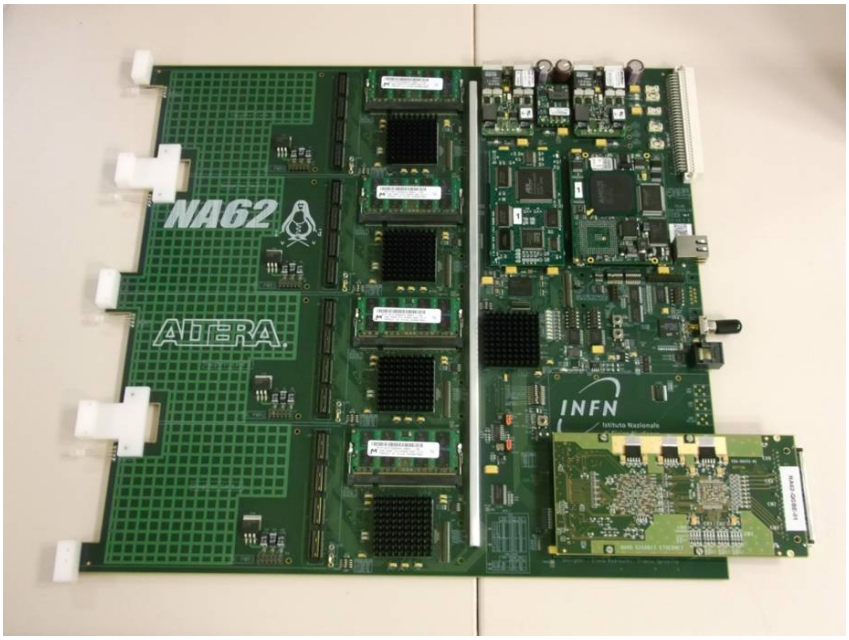

Figure 47: A TEL62 with a TDCB daugtherboard

We first discuss this common system used by CEDAR, CHANTI, RICH, CHOD, LAV, MUV1-2 and MUV3, and partly by SAC and LKr L0 trigger, developed in Pisa.

After several minor changes, the TDCB boards were finalized with version six and a single brand of frontend cables in two flavours for different sub-detectors. 15 additional boards (about 15% of the total) were manufactured and distributed according to sub-detector requests; some minor manufacturing issues had to be solved. The original firmware for these boards was unsatisfactory and not simulated, and was therefore rewritten from scratch during 2012 within the same CAE environment used for the TEL62, allowing a detailed simulation to be carried out, which helped solving several issues. New

important features were implemented, such as a better handling of hit rate fluctuations and an automatic correction for time offsets between different parts of the system, as well as data emulation capabilities which were to be important in the dry run and laboratory tests.

The testing of the first TEL62 version one (V1) prototype did not reveal flaws, and the design of V2 included only very few minor changes, mostly forced by changes in the availability of obsolete components. Pre-production of the 15 boards requested by the sub-detectors for 2012 was delayed as much as possible to allow for more tests: automated testing of the boards by Rome Tor Vergata team was initially foreseen, but the required tools and software could not be ready in time, and the boards had to be manually tested in Pisa before delivery to CERN at the beginning of the dry run.

It should be recalled that the changes between the old LHCb TELL1 board and the TEL62 are quite significant, partly due to the obsolescence of many components used in the LHCb design leading to more powerful devices being used, but also to changes in the overall architecture, first and foremost the use of a large and performing DDR2 dynamic memory for data storage during the L0 trigger latency. The implementation of the firmware in LHCb required a large number of man-years, and while a few concepts from the TELL1 firmware could be reused, most of the TEL62 firmware had to be rewritten from scratch. Unfortunately, the expected involvement of sub-detector groups in the design of the common firmware could not materialize; the Pisa group took over all the missing parts but early in 2012 it became clear that this manpower issue forced to focus on the core implementation of the readout system, postponing the work on the digital trigger part and related inter-board communication. The implementation of the memory handling firmware was found to be particularly challenging, requiring direct intervention of the CAE firm (Mentor Graphics) to fix some bugs in their design tools.

By summer the basic implementation of the readout chain, including data storage and retrieval in the memories, was implemented and simulated, and partially tested at low hit and trigger rates as could be done in the laboratory.

The required quad Gigabit boards (same as on the TELL1 boards) were manufactured in Rome and delivered to CERN at the beginning of the dry run. Testing of the TEL62 boards after installation in ECN3 revealed some fragility, probably related to unsatisfactory component mounting, with some of the boards satisfactorily tested in the lab failing tests after transport to CERN. Most repairs were done on the fly, but this confirmed that the mounting firm will have to be changed for the final production.

TDCB and TEL62 boards were installed on sub-detector systems, and mechanical supports for cabling were developed for this.

An issue arose with the TEL62 crates (Fig. 48): the Collaboration had to adopt a standard manufacturer in order to benefit from CERN support for purchasing, assistance and control software. The crates required a NA62-specific backplane to be manufactured, and while tests on two prototypes did not show any issue, several critical failures appeared on the crates installed in ECN3, proven to be due to manufacturer's fault. These made some systems unusable during the runs, also due to the limited amount of available spares. These issues will have to be pursued thoroughly to avoid breakdown during data-taking runs.

The clock and trigger distribution fibre network was completed right before the start of the dry run. An issue arose in spring with the new production of the TTCex driving modules: the new version of these modules showed a clock phase with an unacceptably high phase instability making the modules unusable for precision clock transmission.

Figure 48: A TEL62 crate cabled up and ready for data taking

Since the problem was not considered to be a fatal issue for the 2012 runs, we managed to obtain from the CERN pool and the CERN PH-ESE group the required number of modules to perform the runs; these modules will be replaced with properly working ones newly built by CERN at the beginning of 2013.

During the dry run a large number of practical issues had to be solved, and the first couple of weeks were spent dealing with basic connectivity issues. This was to be expected, considering that it was the very first time some NA62 installation was taking place in the area, and that heavy refurbishment and ground work was taking place right until the dry run start (actually continuing during the run itself); one of the benefits of the dry run was clearly that it forced many issues to be solved months before the beam period. Several delays were related to the new network system, which involves rather complex routing centrally managed by IT, requiring their intervention for changes as it is not under NA62 control.

As foreseen, the absence of a L0 trigger processor prototype was handled by using the additional functionality of the TALK board, developed by CERN to allow integration of the old readout system of the LKr calorimeter in the new setup, as the new system was not foreseen to be available. With additional firmware effort, the TALK board could effectively act as L0 trigger processor in 2012.

Overall, the experience of the dry run allowed to have a first installation, a successful test of the clock and trigger distribution, and to perform several cycles of TEL62 firmware improvement, as many issues appeared which could not be identified without a full integrated environment with a significant number of channels and a distributed

trigger system. At the end of the dry run we had managed to correctly receive externally generated triggers on the distributed network, store sub-detector pulser data in TEL62 memories and correctly send TEL62-generated data packets to the PC farm, although the complete sub-detector-to-farm data path could not yet be tested fully. The network system was also tested, as well as a very scaled down single-PC version of the readout farm. Trivial but important side results were the finalization of event formats at all levels, with the resulting development of decoding software. The run saw a high participation, with up to 35 people present at some time and regular meetings twice a week. While not all tests which were initially foreseen could be carried out, it was a very significant step forward.

Another significant result was the test of the first prototype Run Control system, implemented by Louvain with CERN support; despite the short time available from the identification of dedicated manpower in spring, the system performed well and represents a significant part of the required final system (Fig. 49). The NA62 version of the software for clock and trigger distribution modules was developed by the Bratislava group and also underwent several cycles of fixing and improvement as issues appeared during the tests with the TALK board and the TEL62.

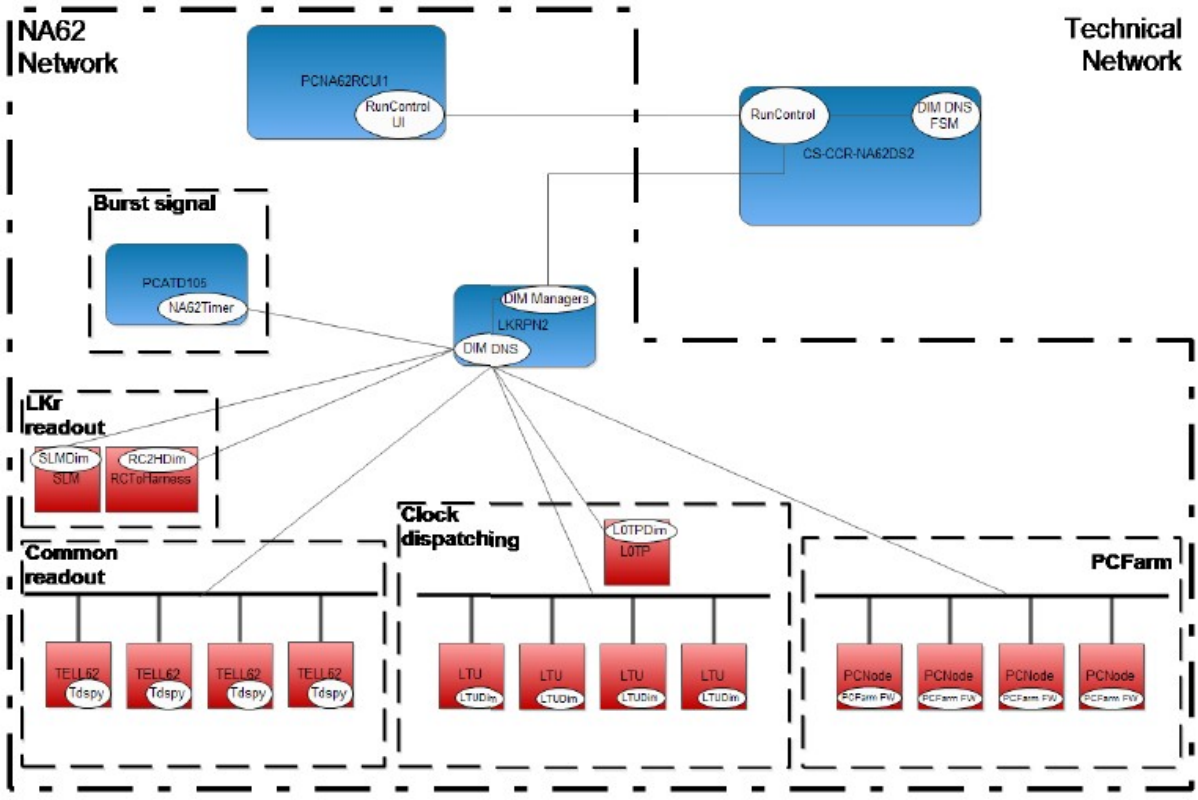

Figure 49: A schematic of the NA62 Run Control

Most of the sub-detectors using the common readout system converged on the adoption of the LAV-FEE board built in Frascati, used also for CHOD, CHANTI and MUV. About 30 of these boards were manufactured and tested in the lab, and installed at CERN in the above systems; the boards worked satisfactorily, not degrading the time resolution, and allowed tests with calibration pulses triggered by the TDC boards during the dry run. The new fast MUV3 trigger detector was connected to the common system through refurbished NA48 constant-fraction discriminator modules built by Turin, and

new translator boards designed by CERN and built in Mainz. The CEDAR successfully tested prototype pre-amplifier boards built in Birmingham.

Concerning other sub-systems, the Straw team read out a few frontend covers with a prototype read out system (SRB) in a stand alone mode. As far as the LKr calorimeter is concerned, a pre-prototype of the CREAM readout module was tested during the TR and prototypes including the required functionalities are expected from CAEN soon. The specifications of the LKr readout cleared the way for the definition of the last missing part of the LKr L0 trigger system, being designed in Rome based on the TEL62. The LKr calorimeter L0 trigger development in Rome Tor Vergata continued with stand alone tests, initially planning for the installation of a single slice system at CERN which could provide simulated data in 2012.

The period between the dry run and the TR was spent in further firmware development, and saw the implementation of a prototype digital trigger TEL62 firmware for the LAV sub-detector, done in Frascati. While, as mentioned, the trigger part was not meant to be tested in 2012, such development prompted further effort in Pisa trying to implement the TEL62 firmware which would allow this part to be also tested. Some studies were also done in Perugia on the digital trigger TEL62 firmware for the CHOD, but these could not go past the simulation level in time for the runs.

Studies on the possible implementation of a PC-based L0 trigger processor continued in Ferrara, with no show stoppers appearing in the measurements of transfer time fluctuations for simulated data from a FPGA development board to a PC. Some software interface was developed and timing of trigger decision algorithms were also performed; plans for a partial test of a prototype system in the fall were laid down.

From the TDAQ point of view, the TR in fall took over the testing from the point which was reached during the dry run. At some point no further progress in debugging could be obtained with the limited tools available in the lab, without using the highly distributed system in which synchronization was provided by actual particles crossing multiple detectors. During the first part of the run the sub-detector collected data using the TEL62 boards in a standalone way, with no triggers; this allowed first checks on the detectors to be done while the investigation of issues in the firmware of the TEL62 and TALK boards allowed to move towards the readout of data with common triggers. This was eventually achieved, although issues remained preventing tests to significantly higher trigger rates, which were always below 100 kHz, one order of magnitude less than the design value.

The common TEL62 firmware for the trigger part was eventually completed in Pisa, and some limited and partial test of the L0 trigger primitive generation firmware developed in Frascati for LAV was also performed at the end of the TR, and will be pursued in the next months as planned. One important result of this activity was to get information on the additional amount of FPGA resources required for a real sub-detector specific firmware: in the specific case of the LAV, while the design still fits within the available resources, this led to considering the possibility of upgrading to higher capacity devices (just a cost issue) for the final production; a decision should be taken early in 2013.

Shortcomings in the test of the common TDAQ system during the TR were the limited data and trigger rate which could be reached and the use of a traditional "old-fashioned" single-level hardware trigger instead of the final multi-level fully digital one, both points related to the development state of the firmware. This implies that we could not yet reach a full assessment on the validity of the current design for the final 1 MHz L0 trigger rate, and although indications are positive this is clearly one of the major and most pressing

goals for the forthcoming months, requiring a significant improvement of high-stress test laboratory setups. Despite the above limits, the fact that we managed to collect hundreds of GBytes of valuable sub-detector data using a completely new data acquisition system (which was the only available system with no back-up) is clearly a major achievement for NA62.

The other obvious limit of the 2012 runs is that several TDAQ sub-systems (LKr, LKr L0 trigger, Straws, GTK, SAC, L0TP) were not really available for testing in an integrated NA62 environment, and these will require thorough testing in 2013, both in the lab and in ECN3.

As planned, the LKr calorimeter was readout during the TR by using the SLM readout system: the interface of this to the new infrastructure was provided by the TALK board built for this purpose: the system worked fine, and its rate limitations were not actually an issue given the relatively low trigger rate achieved. A pre-prototype board of the new LKr readout was installed in the very last day of the run, to obtain some measurements useful for a feedback to the design. The LKr L0 trigger prototype slice and the partial prototype of L0 trigger processor could not be tested at all during the 2012 runs.

All the above issues point to the strong need for more dry runs, as the experience of 2012 showed that these are crucial to achieve significant progress, also due to the identification of issues which only appear in a complex integrated environment. In parallel to this, laboratory test systems will have to grow and become capable of stressing the systems in ways which are closer to what can be done at the experiment.

Concerning the common system, an assessment of the TDC boards is expected by sub-detector groups in early 2013, and production could start by summer. The finalization of the common TEL62 firmware and its test setup is being pursued with highest priority in Pisa to reach a similar assessment for the entire system, in view of a production by the end of the year. Firmware development and testing remain the most urgent issues, and active work should start on the TEL62 trigger firmware for the other sub-detectors involved in L0, namely RICH, CHOD and MUV3.

Some more issues on the common system still stand and could not be fully solved or addressed by the responsible groups, including aspects of rather different relevance such as the instability of the firmware upgrade procedure in the field, pursued by Perugia, the crate malfunctioning issue, and the assessment of the radiation tolerance of the TDAQ system: on the latter, a parasitic study was attempted by the Birmingham group during 2012 in the COMPASS beam, but could not be pursued completely and will require a different approach.

The development of the readout systems for other sub-detectors also saw significant progress during last year, better detailed in the respective sections of this document. Two prototypes for the off-detector readout system for GTK were developed, built and tested in the lab under different conditions; the development of interface boards towards the general NA62 system is well advanced.

While the LAV frontend boards were finalized, produced, tested and used in 2012 for several sub-detectors, new frontend cards for the RICH were also developed (besides those for the CEDAR and MUV already mentioned), all of course compatible with the standard TDC system.

Tests of connections between the prototype LKr readout module and the LKr trigger system are foreseen in the first half of 2013, while the existing backend part of the LKr trigger system should be tested independently; actual implementation of the firmware for this system should also result in further input on the best FPGA size for the TEL62

boards. A detailed Monte Carlo simulation of the LKr L0 trigger is also due and expected soon.

In recent months some progress on the definition of a readout system for the SAC was made in Frascati: this system will also be based on the TEL62, but due to the high rate and limited number of channels it would benefit from a continuous sampling flash ADC readout, rather than a hit-based TDC system. A partially commercial solution is being considered, which would only require to develop some data transfer interface to the common TEL62 system to exploit the standard infrastructure; some data was collected parasitically with the MUV2 system during the TR, in order to check the feasibility of this scenario.

Finally, the L0 trigger processor remains on the critical path: the partial involvement of two groups (Ferrara and Torino) on the PC-based solution led to some progress on measurements of hardware-to-PC data transfer times as well as some first assessment on the software primitive matching algorithm timing; a project for the hardware part of this device, which could be entirely based on commercially available high-speed FPGA development cards appears to be taking off now.

Mention of a significant side-project is also required: the work of an innovative GPU-based L0 trigger started in Pisa raised interest, leading to the involvement of a new group from Rome, with expertise in high-speed communication and parallel computing. With some additional contribution from CERN, this resulted in the setting up of a parasitic system in ECN3 which already underwent partial testing during the TR. While this development is not in the main line of the NA62 TDAQ, further tests in 2013 might show it to be a possible replacement or upgrade for the hardware-based L0-generating implementation, for some sub-detector.

Next year should see the finalization of the common TDAQ system which - barring unexpected issues in tests at the maximum specified trigger rate - should largely be firmware work. Full production of the TDCB cards can start as soon as all sub-detectors give the green light according to their specs and the analysis of technical run data. Some minor changes for the final version of the TEL62 board, related to obsolescing components, are being addressed now are not expected to be an important issue. If the full rate tests are satisfactory, TEL62 production should start within 2013, leaving time for testing and installation in the first half of 2014. Integration tests with the readout systems of other sub-detectors (mainly LKr, GTK, Straw) should be performed in 2013 before production approval of such systems.

On the trigger side an even more intense activity must be carried out, which besides sub-detector specific TEL62 firmware work would see the implementation of inter-board communication for L0 trigger systems distributed over more boards (e.g. RICH), hardware tests of the LKr L0 trigger system communication with the new LKr readout.

The development of the L0 trigger processor still requires a significant effort: if all the studies and measurements do confirm the validity of the current PC-based concept, the activity will involve further development of the interface card firmware, in Ferrara, for Gbit data handling, the development of two small ancillary daughter-cards for interfacing to the experiment (clock and L0 trigger network on one, choke signals from sub-detectors on the other), in Torino, and the development of the L0 primitive matching software.

Summarizing, the most urgent and critical issues for TDAQ remain:

- the assessment of the existing common TDAQ system at full rate;
- the need for a significant involvement of sub-detector groups in the development of

readout and trigger firmware for their system;

- the development of test and quality checking systems for the full productions of TDCBs and TEL62 boards;
- the study, simulation and implementation of high-level software triggers (largely missing);
- the implementation of the L0 central trigger processor. The speed at which these issues can be addressed continues to be limited by the amount of available man-power.

14 $K^+ \to \pi^+\pi^0$ Analysis using the Data from the TR

The test of the response of the sub-detector systems using pure kaon decays was an important goal of the 2012 NA62 TR. The analysis presented in the following sections aims to select $K^+ \to \pi^+\pi^0$ events. Such a sample gives the possibility to test the response of the detectors to pions and photons, to study the timing correlation between the sub-detectors and to investigate the related activity in the veto detectors, namely the LAV stations and the MUV3. The analysis makes use of the data collected during a short data taking run. The trigger requested: an energy deposition in the Neutral Hodoscope (NHOD) and at least one coincidence (Q1) between two quadrants of the Charged Hodoscope (CHOD). The first condition tagged events with an energy deposition in the LKr calorimeter without using any information from the ionization signal of the LKr itself; the second condition selected events with at least one track in the detector acceptance. The CEDAR, two stations of LAV, the CHOD, the LKr, the MUV2 and the MUV3 were readout in this run. The CEDAR was tuned to detect only the Kaons. The average beam intensity was 1/50 of the full one. About 8×10^6 triggers have been collected in this run subdivided in about 450 bursts. About 10% of bursts have been rejected because of data corruption due to readout problems. The selection scheme is the following:

- identification of at least two clusters in the LKr compatible with an electromagnetic-like energy deposition;
- reconstruction of the π^0 four-momentum by looking at all the possible decay vertexes of the event formed by each pair of LKr clusters in the hypothesis of the π^0 mass;
- reconstruction of the π^+ by using the π^0 four-momentum previously reconstructed and the K^+ four-momentum defined at the percent-level by the beam constraint itself.

As a result the $K^+ \to \pi^+\pi^0$ events exhibit a peak in the missing mass distribution, $m^2_{miss} = (P_K - P_{\pi^0})^2$, corresponding to $m^2_{\pi^+}$.

14.1 Identification of the electromagnetic-like clusters in the LKr

A 64×64 cell region of the LKr around the beam hole was readout. A zero suppression was enforced during the run: the shaped signal in each cell was digitized at 40 MHz

and 8 samples were considered; only those cells with a minimum difference of 20 counts between two ADC samples were readout. This zero suppression algorithm differed from the one used during the 2007 run. Fig. 50 shows the average digitized pulse shape (a) and the illumination of the LKr cells (b). The peak of the signal is between samples 4 and 5, while the the first two samples are used for pedestal computation. The small holes in the illumination pattern correspond to not working cells. Their number was substantially unchanged with respect to the 2007 run. The missing columns in the up central part and in the left bottom side are due to hardware problems which have been fixed after the run.

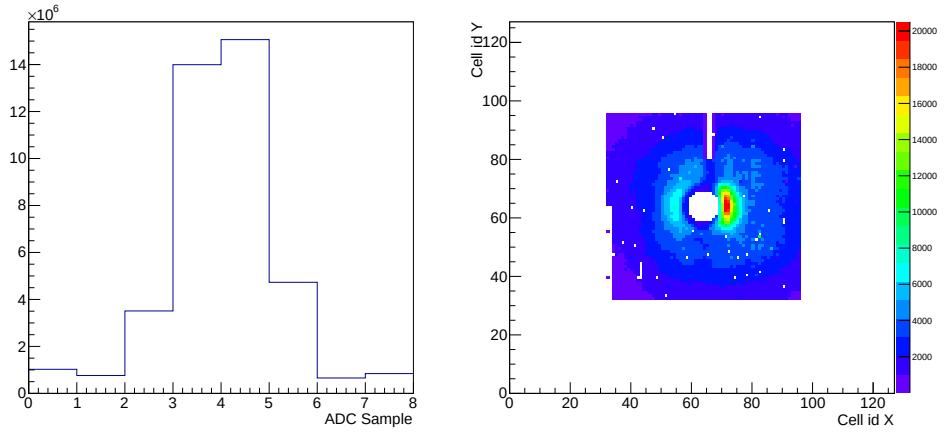

(a) (b)

Figure 50: (a) Digitized cell pulse shape. (b) Illumination pattern of the readout cells. The entries of each cell are weighted with the corresponding energy

The reconstruction of the LKr borrowed the calibration constants and the clustering algorithm from the 2007 run of NA62. Further corrections have been applied to the reconstructed cluster energy in order to take into account the new zero suppression algorithm. The comparison of the energy of the clusters reconstructed in a sample of raw data collected during the 2007 run and processed offline by applying or not the new zero suppression algorithm allowed the extraction of the correction factors. Fig. 51 provides the distribution of the number of cluster reconstructed and the energy of the cluster. The sharp edge at 75 GeV reflects the energy of the beam.

Muons or charged pions release energy in the LKr via ionization, leading to minimum ionization particle (MIP) clusters; photon or electron give electromagnetic clusters; a fraction of the charged pions interacts in the LKr releasing a hadronic shower.

Electromagnetic clusters are selected among those clusters with at least 3 GeV. They have to be reconstructed at least 6 cm away from the lateral sides of the readout region and from the not working region in the central upper part. A cluster must be at least 20 cm distant from any another cluster. The last two requirements allow the selection of the clusters with the best energy resolution. The correlation between the number of cells making up a cluster, N_{cells}, the energy of the cluster, $E_{cluster}$, and the energy of the seed of the cluster, E_{seed}, allow a clean discrimination of the cluster type. The zero suppression algorithm induces an almost linear correlation between $E_{cluster}$ and N_{cells}, with different slopes for hadronic and electromagnetic shower for clusters with more than 20 cells, as

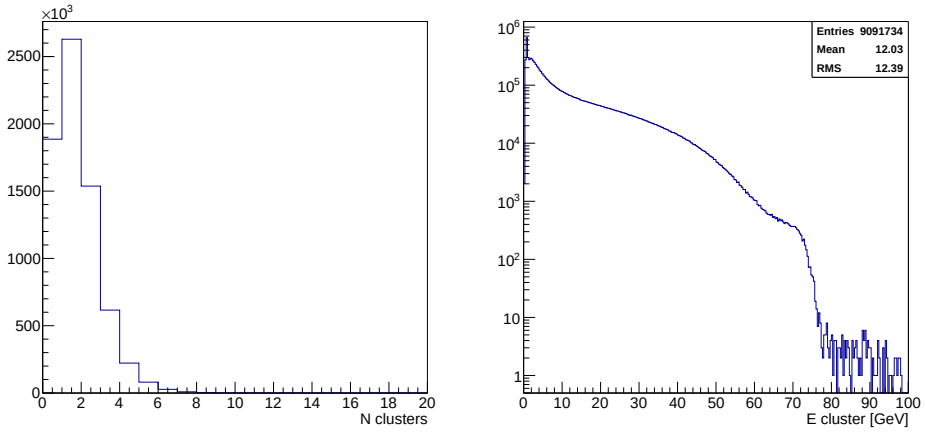

(a) (b)

Figure 51: (a) Number of clusters; (b) energy of the reconstructed clusters

shown in Fig. 52 (a). Similarly the seed of electromagnetic clusters takes away a fraction of energy larger than the seed of hadronic showers. As a consequence an appropriate combination of those variable is exploited in order to select the electromagnetic-like clusters. Fig. 52 (b) shows the distribution of the time difference between the electromagnetic-like clusters of the same event. Only events with at least two electromagnetic-like clusters

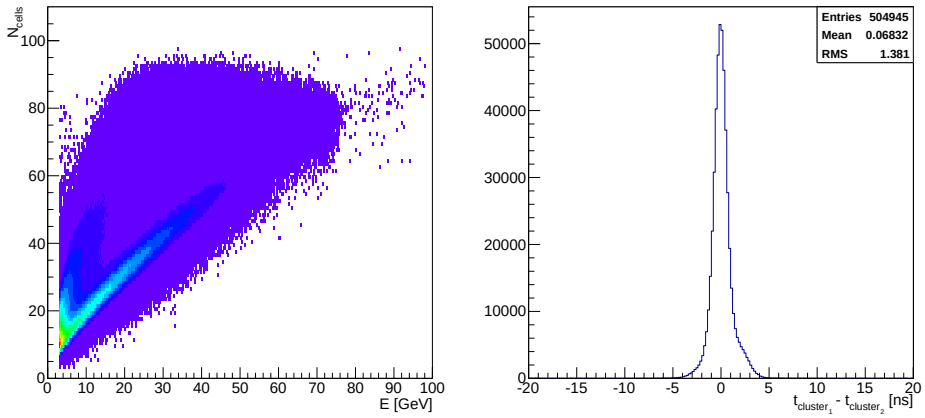

(a) (b)

Figure 52: (a) Number of cells making up a cluster as a function of the cluster energy. (b) Time difference between a pair of electromagnetic-like clusters. The shoulder above 1.5 ns suggests the presence of a residual component of hadronic showers in the selected clusters. The resolution of the peak, excluding the shoulder from the gaussian fit, is about 700 ps (standard deviation)

within ± 1.5 ns in time are considered.

14.2 Reconstruction of π^0

The Z position of the decay vertex, Z_{vertex}, is reconstructed from all the possible pairs of the electromagnetic-like clusters. Under the hypothesis that the observed clusters come from the photons produced by the decay of the π^0, Z_{vertex} can be computed as:

$$Z_{vertex} = Z_{LKr} - \frac{\sqrt{E_1 \cdot E_2 \cdot d_{12}^2}}{m_{\pi^0}}. \quad (1)$$

Here Z_{LKr} is the position of the LKr, E_i are the energies of the clusters, d_{12} the distance between them and m_{π^0} the π^0 mass. A π^0 candidate is a pair of clusters giving Z_{vertex} within 5 and 80 m from the final collimator. The coordinate X_{vertex} is computed from Z_{vertex}, taking into account that the average slope in X direction of the beam entering in the decay volume is 1.2 mrad and that the bending of the beam starts just in front of the final collimator. No displacement, instead, is considered for the Y_{vertex} coordinate. The knowledge of the vertex position and the energy of the clusters allows the reconstruction of the four-momenta of the photon candidates and, hence, of the π^0. Only events with one π^0 candidate are retained. The average of the time of the two photons provides the time of the π^0.

14.3 Kaon

The beam line provided a secondary beam at 75 GeV within 1% momentum bite. Therefore an energy of exactly 75 GeV is assigned to the kaon. The four-momentum of the kaon, P_K, is computed assuming a slope in X direction of 1.2 mrad (from the nominal p_T kick of TRIM5) starting from the final collimator. No slope is considered along the Y direction. The coordinates of the vertex give the position of the kaon at the decay.

14.4 Reconstruction of π^+

Under the hypothesis of a $K^+ \to \pi^+\pi^0$ event, the four-momentum of the π^+ follows from the momentum conservation: $P_{\pi^+} = P_K - P_{\pi^0}$. As a consequence of these assumptions, m^2_{miss} is m_{π^+} in $K^+ \to \pi^+\pi^0$ events. The vertex coordinates give the position of the π^+ at the production. The expected impact point of the π^+ on the various subdetectors can easily be computed by taking into account the 270 MeV/c transverse momentum kick provided by the magnet MNP33 of the spectrometer. Events with the π^+ in the beam hole at the level of the CHOD, LKr and MUV3 are rejected. Only events with the π^+ within the CHOD and MUV3 acceptances are taken into account. Finally an event is discarded if the distance between the impact point of the π^+ on the LKr and one of the photon clusters is less than 20 cm. Fig. 53 (a) shows the distribution of m^2_{miss}. A peak corresponding roughly to the m_{π^+} is clearly visible. Events like $K^+ \to \pi^+\pi^0\gamma$, $K^+ \to \pi^+\pi^0\pi^0$, $K^+ \to \pi^0\mu^+\nu$, $K^+ \to \pi^0 e^+\nu$ and $K^+ \to \pi^+\pi^0$ with the charged pion or an accidental cluster mis-identified as photon cluster, are the main sources of background.

14.5 Analysis of the Selected Events

A candidate in the CEDAR detector is reconstructed by grouping the fired photomultipliers (hits) in a 5 ns time window. The photomultipliers have been previously aligned

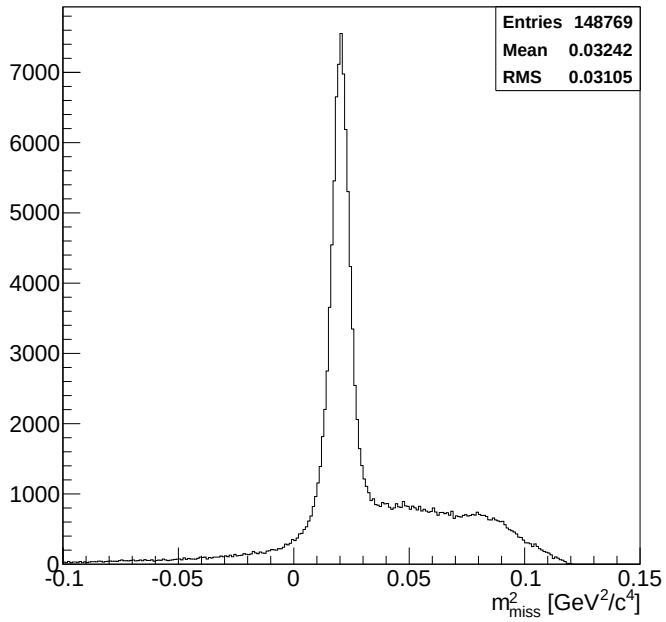

Figure 53: Distribution of the m^2_{miss} for the selected events

in time and corrected for slewing. The time of the candidate is the average time of the hits. A good candidate must have hits in at least 3 sectors. Fig. 54 a) shows a correlation between the time of the π^0 and the time of the CEDAR candidate closest in time to the π^0. The gaussian σ of the time distribution is about 360 ps. A *kaon candidate* is defined as the CEDAR candidate closest in time to the π^0 within ± 3 ns from the π^0 itself.

The time measurement of the CHOD counters have been preliminarily corrected for slewing, impact point position and have been aligned using muons from runs triggered by Q1 only. A CHOD hits is the coincidence between a pair of fired scintillators belonging to corresponding quadrants in the vertical and horizontal planes. The time of the hit is the average of the times of the two counters. A CHOD hit can be correlated in space with the expected impact point of the π^+ on the CHOD with a resolution of few centimeters. The difference between the time of the CHOD hit closest in space to the π^+ and the time of the CEDAR is shown in Fig.54 (b). A very strong correlation is observed between the two detectors. The time resolution is about 400 ps (gaussian σ of the peak). The tail at low values of the time difference is due to events with a high multiplicity in the CHOD. A *pion candidate* is defined as a hit closer than 15 cm from the π^+ impact point position. A further requirement of ± 5 ns from the CEDAR candidate closest in time to the π^0 is applied for those events with only one CHOD hit.

The muon candidates are reconstructed by looking at all the MUV3 pads with signals in both photomultipliers. The maximum between the two time measurements is assigned as the time of the muon candidate, in order to take only the signal produced by scintillation light. The different pads have been aligned in time using muon runs, as for the CHOD. About 10% of the events show a muon activity both in time and out-of-time with respect to the CEDAR (Fig. 54 (c)). This is consistent with the expectations, since a possible decay of the π^+, a punch through from the MUV2 or accidental muons, may produce signals in MUV3. The time resolution of the MUV3-CEDAR difference is about

500 ps (gaussian σ). An *in-time muon candidate* is defined as the MUV3 hit closest in time to the π^0, within ± 5 ns from the corresponding CEDAR candidate.

A MUV2 cluster is reconstructed by considering the time and position of the fired counters in one event and weighting on their energy to get the time and position measurements of the cluster. The MUV2 counters have been previously aligned in time. Fig. 54 (d) shows the difference of the time of the MUV2 cluster and the time of the CEDAR candidate closest in time to the π^0. The distribution exhibits a correlation with the CEDAR candidate, consequence of the showering of the π^+. The time resolution is of the order of 3.5 ns.

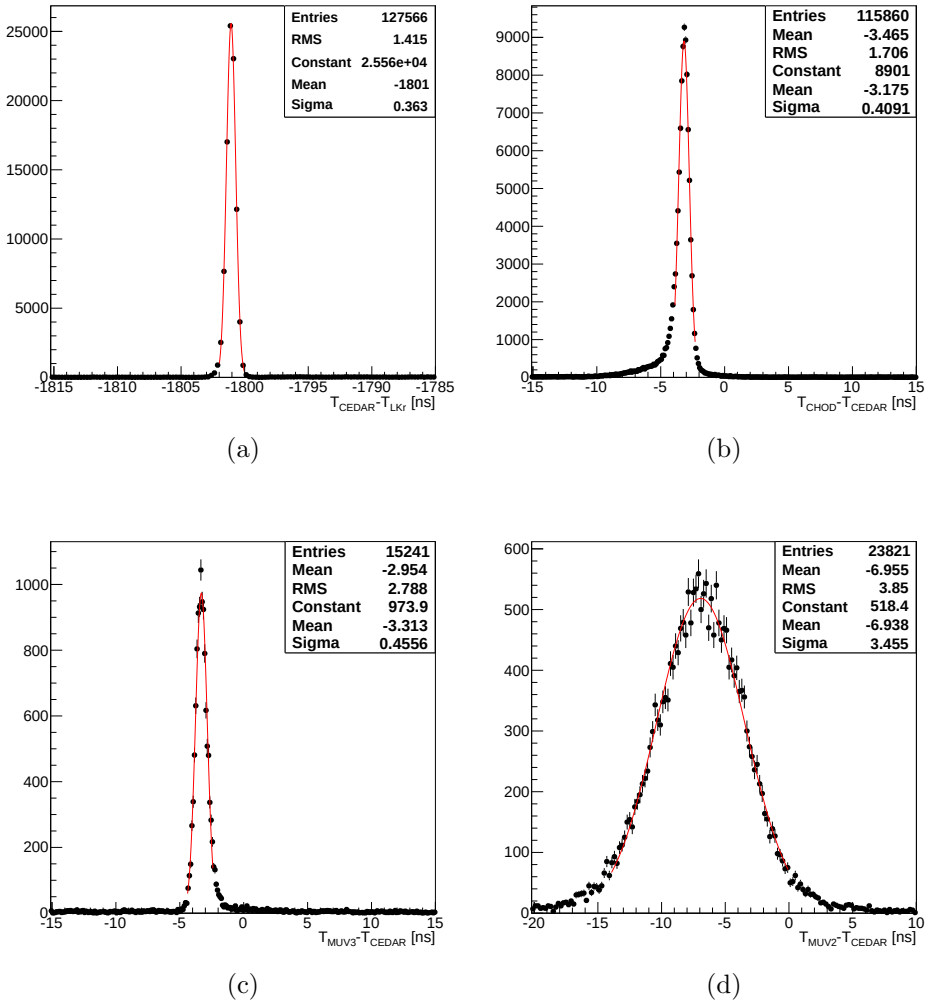

Figure 54: Time difference between the time of the CEDAR candidate closest in the time to the π^0 and (a) the time of the π^0; (b) the time of the CHOD hit closest in space to the π^+ impact point position; (c) the time of the MUV3 candidate closest in time to the CEDAR candidate; (d) the time of the MUV2 cluster

The presence of an extra cluster in the LKr close to the expected π^+ position gives a powerful constraint to further suppress the background. A cluster is associated to the charged pion if it is less than 15 cm distant and is within ± 3 ns from the π^0. Fig. 55 a) and b) show the impact of this request on the background. However, only events with the

π^+ in the acceptance of the LKr can profit from this constraint and the small acceptance of the LKr during the run strongly reduces the number of events where to look for a pion cluster. Nevertheless, the requirement of having a *pion candidate* provides a similar

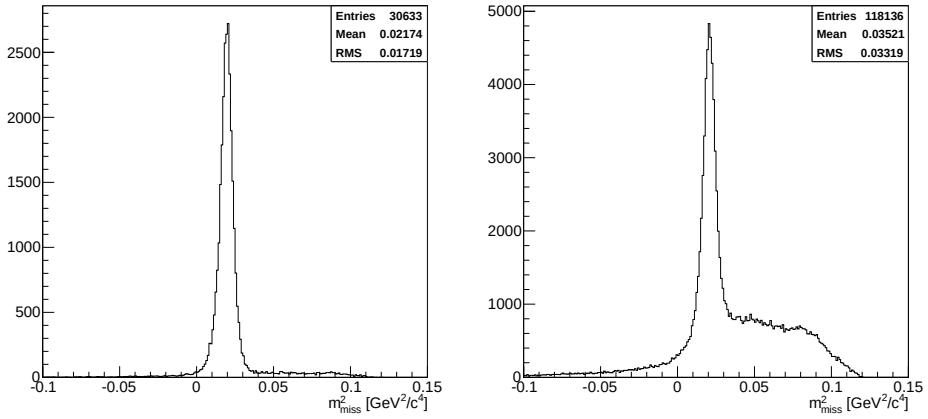

(a) (b)

Figure 55: Distribution of the m^2_{miss} for events with a) and without b) a cluster in the LKr associated to the π^+

background rejection power for those events without π^+ cluster in the LKr.

As a consequence, the events without *pion candidates* are rejected. Among the events with the π^+ in the LKr acceptance only those with a cluster associated to the π^+ are considered. In addition the presence of a *kaon candidate* and no *in-time muon candidates* are required. Figure 56 (a) shows the distribution of the m^2_{miss} of the selected events. The background is less than 10% over the overall mass spectrum, corresponding to a percent level under the peak. The position of the photon clusters and of the expected impact point position of the π^+ for events with $0 < m^2_{miss} < 0.04$ GeV^2/c^2 are depicted in Fig. 56 b) and c), respectively. A gaussian fit to the m^2_{miss} gives an average value of 0.0198 ± 0.0003 GeV^2/c^4 with a resolution of 3.8×10^{-3} GeV^2/c^4. The average value has to be compared with $m^2_{\pi^+} = 0.0195$ GeV^2/c^4. It varies by about 2.5% as a function of the energy of the least energetic cluster, suggesting a residual mis-calibration of the LKr to be accounted for.

The mass region $0 < m^2_{miss} < 0.04$ GeV^2/c^2 defines the sample of $K^+ \to \pi^+\pi^0$. These events allow the evaluation of the efficiency of the sub-detectors. The CEDAR efficiency is about 87 %. This value is consistent with the requirement of hits in at least three sectors over a total of four sectors instrumented during the run. By selecting only the events with a LKr cluster associated to the charged pion, the CHOD efficiency is about 95%. The bulk of the inefficiency comes from the loss of the trailing edge in the TDC readout system. The in-time accidental activity in the MUV3 is about 6%. By neglecting the MUV3 inefficiency, this probability can be considered as an upper limit to the pion loss because of punch-trough in the MUV2. The presence of the MUV1 in front of the MUV2 in the future runs will further reduce this effect. The high inefficiency is entirely due to the 75 ns readout window which does not match the full dynamic range of the MUV2 signals. This problem will be cured in the final version of the readout system.

A first look to the LAV data suggests a 3 % activity associated to the $K^+ \to \pi^+\pi^0$

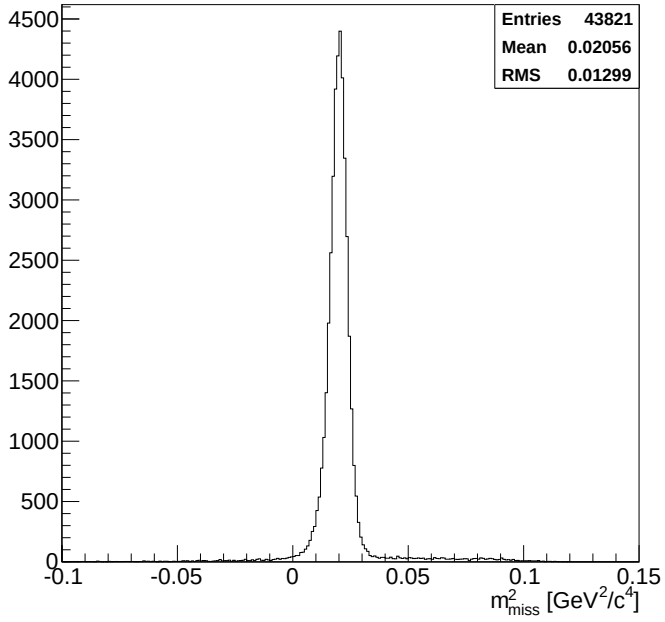

(a)

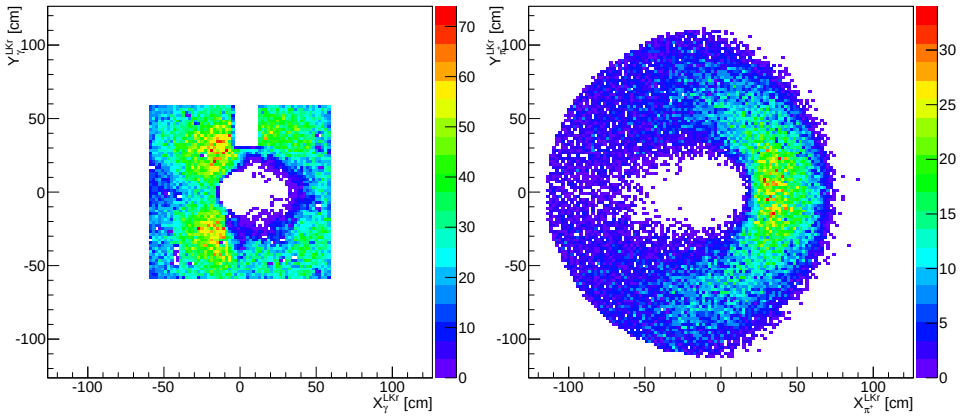

(b) (c)

Figure 56: a) Distribution of the m^2_{miss} for the events selected after all the cuts. Position of the b) photon clusters and of the c) impact point position of the π^+ for events with $0 < m^2_{miss} < 0.04$ GeV^2/c^2

events, integrated over the first two stations and distributed within the 75 ns readout window. The time distribution of the hits does not show any activity in-time with the π^0. The analysis of the LAV data is still on-going.

15 Analysis of MIPs in the LKr using the Data from the TR

The analysis of the MIP-clusters has been performed on the same run used for the $K^+ \to \pi^+\pi^0$ analysis. In order to select a pure sample of minimum ionizing particles, events with exactly one muon candidate in MUV3 are considered. A further requirement of having at least one hit reconstructed in the CHOD, matching in space and time the muon candidate, allows the selection of muon candidates passing through the LKr acceptance. The MIP-cluster candidate is defined as the LKr cluster closest to the CHOD hit. This cluster has to be reconstructed within 10 cm from the CHOD hit and it has to be in time with the CHOD hit within $\pm$ 6 ns. The energy distribution of the selected clusters exhibits a peak at 500 MeV, as shown in Fig. 57 (a), well described by a convolution of a Landau and a Gaussian function. The average value is also in agreement with the expected ionization loss from minimum ionizing particles in LKr. In most cases these clusters are formed by less than 10 cells (Fig. 57 (b)).

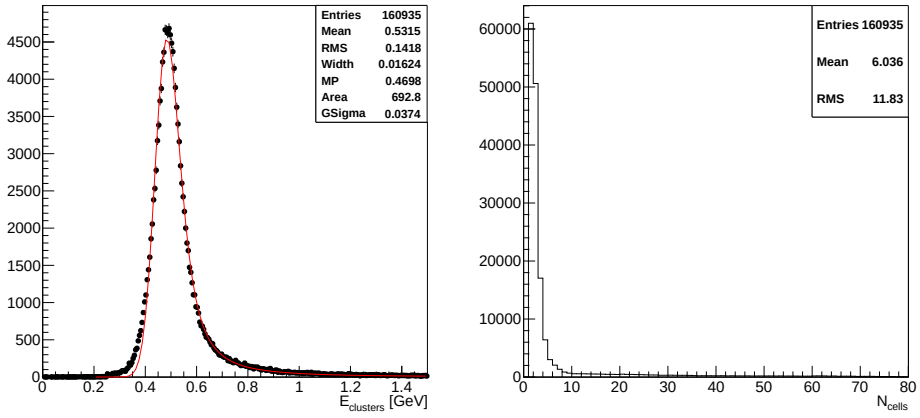

(a) (b)

Figure 57: a) Energy distribution of the MIP-clusters. The fitting function is the convolution of a gaussian and a landau. The most probable value of the landau (MP) is 470 MeV, the σ of the resolution function is 37 MeV, well in agreement with the noise effect expected on clusters of 5-6 cells. b) Number of cells forming a MIP-cluster

Taking into account the above observations, it is possible to select MIP-clusters independently from other detectors, by requiring less than 10 cells in the LKr and energy between 400 and 650 MeV. Fig. 58 shows the position of MIP-clusters selected using the LKr only in the same run used for the $K^+ \to \pi^+\pi^0$ analysis. The hot-spot region close to the beam hole originates from the muons produced by the decays of the pions in the beam. Because of the Q1xNHOD trigger used in the analyzed run, these muons could only be readout accidentally together with the main event. A deposition of a minimum

ionizing particle alone does not fulfill the NHOD condition. By assuming 75 ns as an effective LKr readout window for a reconstructed cluster (3 central samples out of the 8 samples), the extrapolated rate of MIP-clusters at full intensity in a 8×8 cm^2 region around the hot-spot is about 1.5 MHz, corresponding to about 100 KHz in the two most populated cells. This is the hottest region in LKr expected at full intensity.

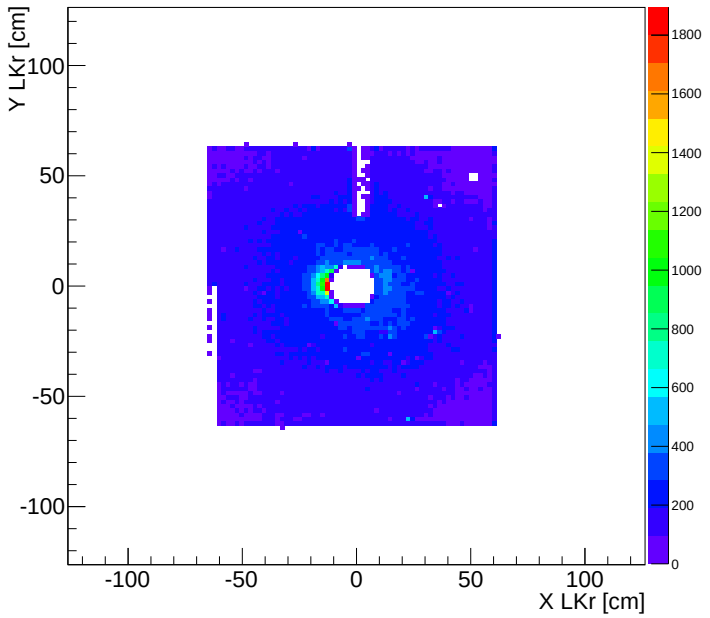

Figure 58: Position on the LKr of the clusters made up by less than 10 cells and with a reconstructed energy between 400 and 650 MeV

16 Conclusions on the TR analysis

The analysis of the data from one run collected by NA62 during the technical run allows the selection of a pure sample of more than 4×10^4 $K^+ \to \pi^+\pi^0$ with a percent level background. A clear timing correlation is present between the various subdetectors, showing time resolutions for the LKr, the CEDAR, the CHOD and the MUV3 below 500 ps. The efficiency of the CEDAR, CHOD and MUV2 are well under control. The measured inefficiencies are in agreement with the expectations and are mostly linked to the partial configuration of the detectors and readout system adopted during the run. The out-of-time activity in the LKr and MUV3 due to the beam seems also in agreement with the expectations. The $K^+ \to \pi^+\pi^0$ is not suitable for measuring the efficiency of the LAVs and the MUV3. They are under study using different methods together with the accidental activity in the LAV stations.

The CHOD and MUV3 provide a sample of muons, useful to highlight the LKr capabilities in detecting MIPs. This also allows an estimation of the expected rate at full intensity in the hottest region of the LKr.

17 Publications and analysis of older data

The principal goal of the NA62 physics programme based on the 2007 data set was the precision measurement of the helicity suppressed ratio of the leptonic decay rates $R_K = \Gamma(K^\pm \to e^\pm\nu)/\Gamma(K^\pm \to \mu^\pm\nu)$. This dedicated effort is now completed, with the publication of a result based on a partial data sample [18] followed by a recent publication of the final result based on the full data sample [8]. The result $R_K = (2.488\pm0.010)\times10^{-5}$ has a record precision of 0.4% and agrees with the SM prediction $R_K^{\rm SM} = (2.477\pm0.001)\times 10^{-5}$.

A distinctive feature of the NA62 2007 data sample is a relatively low intensity beam and minimum bias trigger conditions used. This uniquely allows measurements of a number of rare $K^\pm$ decays that are difficult to address in conventional experiments with selective triggers, despite the modest $K^\pm$ flux collected ($\sim$ 10 times lower than of the NA48/2 experiment).

The $K^\pm \to \pi^\pm\gamma\gamma$ rare decay analysis became the first to report preliminary results in 2012. The predictions of the Chiral Perturbation Theory (ChPT) for the decay rate and spectrum have been validated, and the fundamental ChPT parameters were measured with a low-background sample of 175 decay candidates [20]. The analysis was finalized by February 2013, and a publication is in preparation. Other progressing analyses based on the 2007 data set include measurements of the structure-dependent component of the radiative $K^\pm \to e^\pm\nu\gamma$ decay and the searches for long-lived sterile neutrinos ν_H in the $50 - 350$ MeV/c^2 mass range produced via the decay $K^\pm \to \mu^\pm\nu_H$.

Ananalysis of 2003-2004 data (Ke4 Branching fraction and absolute form factor) is finalized and an analysis of hyperon data from NA48/1 has been completed. More analyses of both NA62 and NA48/2 data are in progress and are being presented as preliminary results at conferences.

For convenience, the most recent publications are listed below.

- NA62 Collaboration

  Precision Measurement of the Ratio of the Charged Kaon Leptonic Decay Rates

  Physics Letters B 719 (2013)326 (February 2013)

- NA48/2 Collaboration

  New measurement of the $K^\pm \to \pi^+\pi^-e^\pm\nu$ (K_{e4}) decay branching ratio and hadronic form factors

  Physics Letters B 715 (2012), pages 105-115 (August 2012)

- NA48/1 Collaboration

  Measurement of the branching ratio of the decay $\Xi^0 \to \Sigma^+\mu^-\bar{\nu_\mu}$

  Physics Letters B 720 (2013) 105 (March 2013)

The collaboration is actively contributing to major international conferences and topical workshops with NA62 detector contributions and recently published or preliminary physics results from NA62 and NA48/2. In the past year (April 2012 to April 2013), the collaboration speakers presented 33 contributions to physics conferences and 20 contributions to instrumentation conferences. More contributions are foreseen in 2013.

References

[1] A. Crivellin, L. Hofer, U. Nierste and D. Scherer, "Phenomenological consequences of radiative flavor violation in the MSSM," Phys. Rev. D **84** (2011) 035030 [arXiv:1105.2818 [hep-ph]].

[2] J. Brod, M. Gorbahn and E. Stamou, "Two-Loop Electroweak Corrections for the $K \to \pi\nu\bar{\nu}$ Decays," Phys. Rev. D **83** (2011) 034030 [arXiv:1009.0947 [hep-ph]].

[3] A. V. Artamonov *et al.* [BNL-E949 Collaboration], "Study of the decay $K^+ \to \pi^+\nu\bar{\nu}$ in the momentum region $140 \leq \mathrm{P}(\pi) \leq 199$ MeV/c," Phys. Rev. **D79** (2009) 092004. [arXiv:0903.0030 [hep-ex]].

[4] R. Aaij *et al.* [LHCb Collaboration],

[5] R. Aaij *et al.* [LHCb Collaboration], "Evidence for CP violation in time-integrated $D^0 \to h^-h^+$ decay rates," arXiv:1112.0938 [hep-ex].

[6] R. Aaij *et al.* [LHCb Collaboration], "Search for direct CP violation in D0 -¿ h- h+ modes using semileptonic B decays," arXiv:1303.2614 [hep-ex].

[7] J. Adam *et al.* [MEG Collaboration], "New constraint on the existence of the mu+-¿ e+ gamma decay," arXiv:1303.0754 [hep-ex].

[8] C. Lazzeroni *et al.* [NA62 Collaboration], "Precision Measurement of the Ratio of the Charged Kaon Leptonic Decay Rates," Phys. Lett. B **719** (2013) 326 [arXiv:1212.4012 [hep-ex]].

[9] "Cryopump System for NA62 experiment", CERN, April 4, 2012, EDMS 1165399

[10] Edward R. Murphy et al., Solder-based chip-to-tube and chip-to-chip packaging for microfluidic devices, The Royal Society of Chemistry, 2007

[11] "Construction and test of a RICH prototype for the NA62 experiment", G. Anzivino et al, Nucl. Instrument. and Meth. A 593(2008) 314-318

[12] "Pion-Muon separation with a RICH prototype for the NA62 experiment", B.Angelucci et al, Nucl. Instrument. and Meth. A 621 (2010) 205-211

[13] OPAL Collaboration, K. Ahmet *et al.*, Nucl. Instrum. Meth. A **305**, 275 (1991).

[14] F. Ambrosino *et al.*, arXiv:1111.4075 [physics.ins-det].

[15] A. Antonelli *et al.*, JINST **8**, C01020 (2013)

[16] B. Angelucci *et al.*, JINST **7** (2012) C02046.

[17] F. Hahn *et al*, NA62 Technical Design Document, NA62-10-07 (2010).

[18] C. Lazzeroni *et al.*, Phys. Lett. **B698** (2011) 105.

[19] C. Lazzeroni *et al.*, Phys. Lett. **B719** (2013) 326.

[20] E. Goudzovski, Proceedings of the FPCP 2012 conference (Hefei, China, 21–25 May 2012). arXiv:1208.2885.